FOI-R--0163--SE

July 2001

ISSN 1650-1942

Scientific report

Tomas Carlsson, Ove Steinvall, Dietmar Letalick

Signature simulation and signal analysis for 3-D laser radar

Issuing organization	Report number, ISRN	Report type
FOI – Swedish Defence Research Agency Sensor Technology P.O. Box 1165 SE-581 11 Linköping	FOI-R--0163--SE	Scientific report
	Research area code 4. C4ISR	
	Month year July 2001	**Project no.** E7030
	Customers code 5. Contracted Research	
	Sub area code 42 Surveillance Sensors	

Author/s (editor/s)	Project manager
Tomas Carlsson Ove Steinvall Dietmar Letalick	Erland Jungert
	Approved by Svante Ödman
	Scientifically and technically responsible Ove Steinvall

Report title (In translation)

Signature simulation and signal analysis for 3-D laser radar

Abstract (not more than 200 words)

From ordinary laser data you can easily determine the distance to the target in every single laser shot. A development from this original technique is to extract the reflected waveform from every laser shot. The latest addition to this technology is the 3-D laser radar, which gives an array of reflected laser pulse waveforms.

Theories regarding the earlier forms of laser measurements can be, and have been, applied on this latest technology, the 3-D laser radar. Though until this master thesis they have not been gathered in a toolbox in MATLAB and therefore they have not been sufficiently tested and evaluated.

The report contains the theoretical background for the simulation of the reflected waveform and then a validation of the algorithms. To analyze the simulated waveform, this report presents an attempt to use surface classification to detect the slope of a surface.

The toolbox is implemented in MATLAB and is in this report only presented with description.

Keywords

laser, laser radar, waveform simulation, target recognition, toolbox, matlab

Further bibliographic information	Language English

ISSN 1650-1942	Pages 57 p.
	Price acc. to pricelist Security classification

Utgivare Totalförsvarets Forskningsinstitut - FOI Sensorteknik Box 1165 581 11 Linköping	**Rapportnummer, ISRN** FOI-R--0163--SE	**Klassificering** Vetenskaplig rapport
	Forskningsområde 4. Spaning och ledning	
	Månad, år Juli 2001	**Projektnummer** E7030
	Verksamhetsgren 5. Uppdragsfinansierad verksamhet	
	Delområde 42 Spaningssensorer	
Författare/redaktör Tomas Carlsson Ove Steinvall Dietmar Letalick	**Projektledare** Erland Jungert	
	Godkänd av Svante Ödman	
	Tekniskt och/eller vetenskapligt ansvarig Ove Steinvall	

Rapportens titel

Signatursimulering och signalanalys av data från 3-D-laserradar

Sammanfattning (högst 200 ord)

Från vanliga laserdata kan man enkelt bestämma avståndet till målet i varje skott. En vidareutveckling är att extrahera den reflekterade vågformen i varje laserskott. Det senaste tillägget till tekniken är den så kallade 3-D-laserradarn som sveper över målet och genererar en matris av reflekterade vågformer.

Teori från den tidigaste formen av laser har applicerats på den senaste teknologin, 3-D-laserradarn. Innan det här projektet har de dock inte varit samlade i en toolbox i MATLAB och därmed inte tillräckligt väl testade och utvärderade.

Den här rapporten innehåller den teoretiska bakgrunden för simulering av den reflekterade vågformen följt av en mindre validering av algoritmerna. För att analysera den simulerade vågformen, presenterar den här rapporten ett försök att utgående från vågformen identifiera lutningen hos en yta.

Toolboxen är implementerad i MATLAB och framställs i denna rapport endast med en beskrivning.

Nyckelord

laser, laserradar, vågformssimulering, måligenkänning, toolbox, matlab

Övriga bibliografiska uppgifter	**Språk** Engelska
ISSN 1650-1942	**Antal sidor:** 57 s.
Distribution enligt missiv	**Pris: Enligt prislista** **Sekretess**

Notation

Symbols

A_r	Receiver aperture radius.
B	Receiver electrical bandwidth.
$\Delta\lambda$	Receiver optical filter bandwidth.
E_p	Laser pulse energy.
f	Receiver focal length.
F	Receiver excess noise factor.
h_sun	Sun spectral irradiance.
$I(R, r)$	Irradiance distribution.
I_db	Receiver bulk dark current.
I_ds	Receiver surface dark current.
λ	Wavelength.
M	Detector internal gain.
$p(t)$	Time distribution of the laser pulse energy.
P_scint	Probability density function for turbulence scintillation.
P_sp	Probability density function for speckle attenuation.
ϕ	Beam divergence.
Ψ	Aerosol attenuation factor.
Q	Glint-to-diffuse optical power.
R	Mean distance to target.
R_0	Laser focusing range.
$\Re$	Receiver responsivity
ρ_l	Radius of a turbulence cell.
$\boldsymbol{\rho}$	Bidirectional reflection distribution function (BRDF). (Scalar)
ϱ	Reflectance.
$p(t)$	Continuous time function.
$p[t]$	Discrete time function.
$\boldsymbol{\sigma}_\mathrm{aer}$	Atmospheric attenuation. (Scalar)
σ	Standard deviation.
$T_{1/2}$	Laser pulse half width (FWHM).

T_r	Receiver optical transmission.
ϑ_fov	Receiver field of view (IFOV).
$\Theta(t)$	The Heaviside function.
w	Beam diameter.
w_0	Beam diameter at laser source.

Operators and Functions

*	Convolution.
$\square$	Correlation.

Abbreviations

3-D	Three dimensional.
BRDF	Bidirectional reflection distribution function.
CAD	Computer aided design.
FOI	The Swedish Defence Research Agency.
FWHM	Full width at half maximum.
IFOV	Instantaneous field of view.
Laser	Light amplification by stimulated emission of radiation.
Lidar	Light detection and ranging.
NEP	Noise equivalent power.
pdf	Probability density function.

Contents

1 Introduction

1.1 Background

The first *laser* (Light Amplification by Stimulated Emission of Radiation) was developed in the 1960s. The laser beam has special properties making it interesting for several applications. One of the first ideas was to send a pulse towards a target and measure when it arrives back at the receiver. The time gives an approximation of the range to the target in every single laser shot. Over the following decades methods to extract data from that conventional laser measurement have been well developed. On the contrary, the possibilities to determine properties of the surface have been severely restricted.

At the department of Laser systems at the Swedish Defence Research Agency (FOI), research is performed on an image producing and range measuring laser technique, the so called *laser radar*. One of its many advantages is that soft covers are penetrated by the laser which gives the possibility of recognition in spite of camouflage by, for instance, camouflage nets, vegetation or smoke.

The laser radar system generates a time distribution of the reflected energy, which makes it possible to extract properties of the reflected surface, such as the shape and the surface roughness. It is also possible to obtain "ordinary" intensity images as pixel arrays, with distance information in every pixel. The correctness in this measurement varies heavily due to several parameters, such as turbulence, speckle noise, range, angle of incidence to the target etc. Earlier research [4] has given physical models to estimate the error with known noise parameters.

1.2 Objectives

The master thesis consists of two phases:

1. Implementation and evaluation of a MATLAB toolbox (algorithm package) using the physical models to generate a range array image with the reflected waveform in every pixel. This toolbox will be a part of the modeling and simulation tools that have been developed at the department.

2. Exemplifying the use of the toolbox from phase 1 by choosing, implementing and evaluating a target recognition algorithm on some simple targets. An idea is to define typical properties (waveforms from the distance measurement etc.) for some different types of targets and compare these with the measured data from an unknown target.

1.3 Simplifications

The reality is complex, and to simulate every particle in the air and on the target will not be possible. Therefore appropriate simplifications are applied to the models. Most of these are inherited from the references. The simplifications are specified at each point they are applied.

1.4 Thesis outline

Chapter 1 holds the introduction to this master thesis. Chapter 2 treats the theories of 3-D laser radar and the modulation of the laser pulse during the propagation of the wave. In chapter 3 the basic ideas about the implemented simulation are presented. The following chapter contains the validation of the simulation tool. In chapter 5, some theories covering target recognition are treated followed by the results of the tests. Finally, in chapter 7, some discussion about conclusions and ideas of extensions to this work, are presented.

Appendix A contains a description about the implemented toolbox and how to use it. The index in the end of this report contains the most difficult words where **bold** numbers mean the definition of or explanation for the word and *italic* numbers refer to figures illustrating the word.

2 Laser beam propagation theory

This chapter contains a guide into the world of 3-D laser radar. In the beginning of the chapter the general properties of the undisturbed laser beam propagation are described. Both in the time and spatial domain. The following sections treat the modulation of the beam on its way to the target and back to the receiver. This modulation is divided into the target interaction, the atmospheric disturbances, and the receiver properties. The target reflection depends on both the geometric shape and the surface structure of the target. The atmospheric disturbances are divided into beam broadening, intensity fluctuation and attenuation. Finally the receiver introduces noise into the signal depending on the construction of the receiver.

2.1 Laser beam energy distribution

In this section the idealized energy distribution of the laser is described. A pulse propagating in positive z-direction can be described as an intensity in three dimensions $U(x, y, z)$ that approximately can be separated into $U(x, y, z) = I(z) \cdot I(x, y) = I(ct)I(x, y) = p(t)I(x, y)$. In the first part, section 2.1.1, the time propagation, $p(t)$, is described. It is followed by the description of the radial distribution, $I(x, y)$, in section 2.1.2.

2.1.1 Time propagation

The time propagation for a typical laser pulse can be described by

$$p(t) = \left(\frac{t}{\tau}\right)^2 \cdot e^{-\frac{t}{\tau}}, \tag{2.1}$$

$$\text{where} \quad \tau = \frac{T_{1/2}}{3.5},$$

and $T_{1/2}$ is the Full Width at Half Maximum (FWHM), a standard measure of the pulse width. Figure 2.1 shows the time propagation for a typical laser pulse according to equation (2.1). This pulse is a standard pulse used in laser radars, and by controlling $T_{1/2}$, different properties of the pulse can be discovered. The following discussion assumes that the noise level is constant when the momentary signal power varies. Since this is approximately true, we can assume that, the more power the signal contains, the higher Signal-to-Noise-Ratio (SNR) we get. If a short pulse (small $T_{1/2}$) is used, the energy would be concentrated in time and a higher peak power would appear in the received signal, but the received signal might look like noise, and you might fail to detect it. If a long pulse (large $T_{1/2}$) is used instead, the time distribution of the pulse energy

would be smoothed and a lower peak power would appear in the receiver. It may be too low to recognize it due to noise. On the other hand, if the SNR is enough to detect the signal, it is more likely detected as a pulse if the pulse is long.

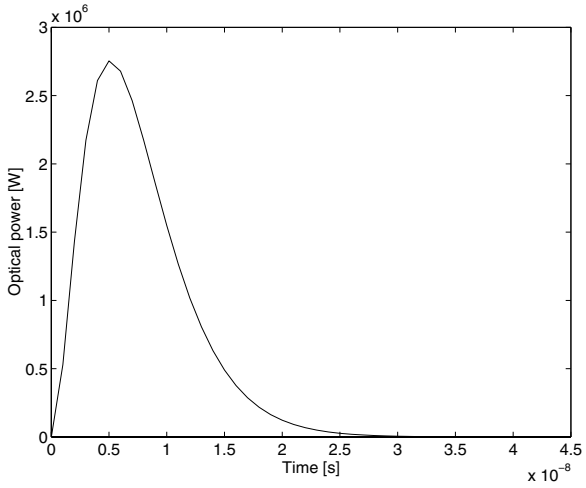

Figure 2.1. The laser pulse with $T_{1/2} = 2\,\text{ns}$.

Another possible problem with long pulses might arise when watching a reflected pulse, while the target consists of two surfaces at different distances. Normally a double pulse would be returned, but if the pulse is too long, these two peaks could cover each other and be detected as only one pulse, and therefore only one surface. Since this is an ordinary way of detecting edges of an object, too long pulses are not recommended.

2.1.2 Irradiance distribution

The irradiance means the amount of energy per time unit and area unit (W/m^{-2}). With irradiance distribution the spatial distibution, $I(x, y)$, of the irradiance is meant. The laser beam irradiance distribution is Gaussian where most energy per unit area is in the center of the beam. Further away from the center, with increasing radius r, the irradiance decreases as e^{-r}, see Figure 2.2.

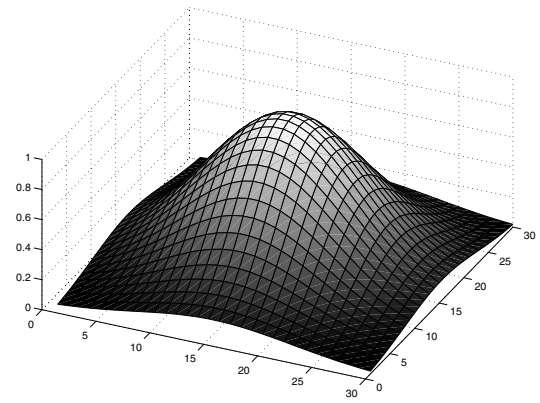

Figure 2.2. The Gaussian irradiance distribution of a laser beam. The energy is concentrated to the center of the beam.

The Gaussian irradiance distribution follows (as described in Steinvall [14]) the expression

$$I(r) = \left(\frac{w_0}{w}\right)^2 \cdot e^{-\frac{2r^2}{w^2}}, \tag{2.2}$$

where w_0 is the beam radius at the laser source and w is the beam radius at a specific distance from the laser source. The beam radius w is defined as the radius r where the irradiance is reduced to $e^{-2}(\approx 0.135)$ of the top value. By integrating equation (2.2) over the laser beam area we receive the total power as

$$P_{tot} = \int_0^\infty I(r) \cdot 2\pi r \, \mathrm{d}r = \frac{\pi w_0^2}{2}. \tag{2.3}$$

The beam radius at range R, see Figure 2.3, is (in free space) given by

$$w = w_0 \sqrt{(\Omega_0^2 + \Omega^2)}, \tag{2.4}$$

$$\text{where} \quad w_0 = \frac{2\lambda}{\pi\phi}, \quad \Omega = \frac{\lambda R}{\pi w_0^2}, \quad \Omega_0 = 1 - \frac{R}{R_0}.$$

In the last equation, R_0 is the focusing range of the laser source. The wavelength of the laser source is λ. The beam divergence, ϕ, is the divergence angle of the beam, see Figure 2.5. Note that the beam width not only depends on the divergence angle ϕ, but also on the focusing range. It causes the beam width close to the laser source to grow, see Figure 2.3.

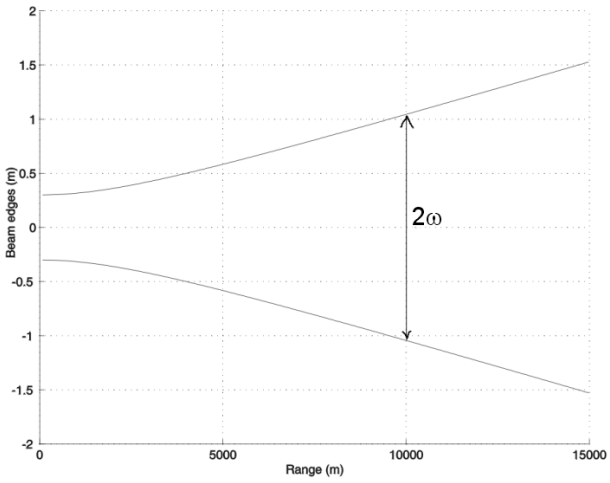

Figure 2.3. Beam sizes as function of range for $\phi = 0.2$ mrad and $R_0 = 3$ km.

2.2 Target interaction

When a laser pulse hits a target it will be reflected into many directions. The slope of the surface is one main factor. Another important factor affecting this reflection is the partition in diffuse and specular reflection. The specular reflection is the reflection with the same angle of incidence as the angle of reflection. The diffuse reflection spreads into all directions, even if the direct (specular) reflected light is in some other direction. See Figure 2.4 for some examples of reflection. Section 2.2.1 treats the reflection and section 2.2.2 the surface properties.

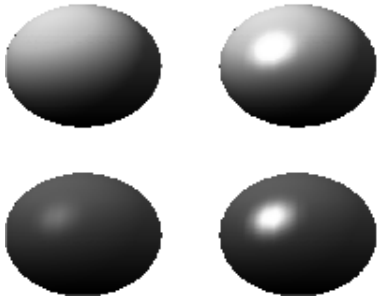

Figure 2.4. Examples of reflection. From left to right we have low and high specular strength. From top to bottom we have strong and weak diffuse reflection, respectively.

2.2.1 Reflection

Reflection induces two main aspects of modulation on a laser pulse. The first aspect is *time independent* pulse reflection. In this mode the focus lies on the directions of the energy of the reflected pulse and the time dependence of the pulse is not considered. Only how much energy that is reflected into the receiver is measured.

The other aspect, *time dependent* pulse reflection, considers the time function of the pulse, and how it is modified when it is reflected at the target. Steinvall [13] describes these two cases further.

Since the target description in this report derives from a CAD model, see section 3.2, spherical surfaces are approximated with plane facets. With the number of facets increasing to infinity the same result as an analytic solution of the reflection will be given. Analytic solutions covering non-planar surfaces such as cones, spheres, paraboloids and cylinders can be found in Steinvall [13].

When a very short pulse, an impulse or a dirac function δ, is sent on the target, the reflected pulse is what is usually called the *impulse response*. With a known impulse response for a target area, the reflected waveform from any pulse sent at the target can be calculated as a convolution between the impulse response and the sent pulse.

The impulse response for a plane surface reflection of a laser beam is described in Steinvall [14] by

$$h(t) = \iint_{-\infty}^{\infty} e^{-\frac{(x-x_0)^2-y^2}{w^2}} \cdot \delta\left(t - 2\frac{L(x,y)}{c}\right) \mathrm{d}x\,\mathrm{d}y \tag{2.5}$$

and in Figure 2.5, where x_0 is the x-value for the target where the center of the beam is reflected and c is the speed of light. To get the impulse response, we convolve (see equation (2.8)) the dirac function, $\delta(t)$, with the pulse.

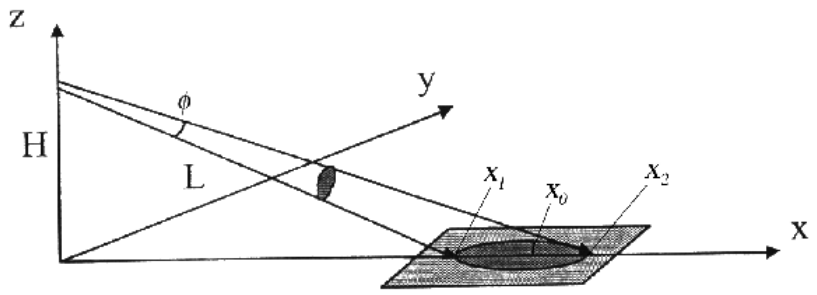

Figure 2.5. The geometry of a plane reflection with a Gaussian distributed beam. The figure is taken from Steinvall [14].

The distance between the target and the receiver in each pixel at position (x, y) is approximated by

$$L(x, y) \approx \frac{x}{\cos \alpha}, \tag{2.6}$$

where α is the angle of incidence (see Figure 2.6) which is the same as the angle of reflection. Normally the angle of incidence is defined as the angle between the surface normal and the incident light, but in this case α is defined as the angle between the incident light and the surface. The approximation that eliminates the variable y is valid because the spot is relatively small in the y-direction compared to the x-direction, see Figure 2.5. Solving the integral (2.5) we find that

$$h(t) = e^{-\left(\frac{t-t'}{\tau_0}\right)^2}, \tag{2.7}$$

$$\text{where} \quad t' = \frac{2x_0}{c \cdot \cos \alpha}, \quad \tau_0 = \frac{w\sqrt{2}}{\sin \alpha}.$$

As in equation (2.7), the time distribution of the impulse response is symmetric around the mean time of the two-way propagation. This is due to the plane reflection and is not applicable for most of the targets.

In the case of simulation the area of a laser beam is divided into a large number of subareas. In this way the assumption can be made that each subarea of the laser beam is reflected on a plane surface and that complex target surfaces consist of a number of plane surfaces. Therefore, no theories of reflection for other targets than plane surfaces are needed. The assumption that the energy distribution of the laser beam inside each subarea is constant is also made, see Figure 2.2. The larger number of subareas, the better approximation we achieve.

Since the impulse response above is calculated with a laser beam of Gaussian energy distribution, this is not suitable for the simulation. As stated above, the assumption is made that inside each subarea the beam energy distribution is constant and the shape is a square. Therefore, another impulse response has to be used.

Algorithm 1 describes a way of calculating the reflection for a random target. The assignments used in the algorithm below refer to Figure 2.6.

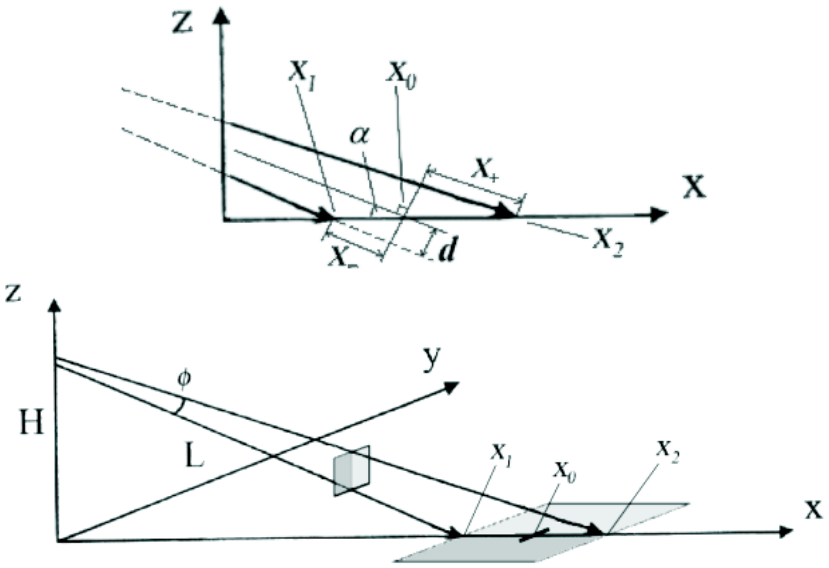

Figure 2.6. Top: a detailed description of the variables used in the creation of the impulse response. Below: a more common description of the geometry with a square shaped surface reflection.

Algorithm 1 (Reflection calculation)

Step 1: *The assumption is made that the irradiance distribution of the beam is constant (and of the shape of a square) inside the subarea.*

Step 2: *The simplified calculation assumes that the reflection is made perpendicular to the y-axis, which is not correct, but a good approximation. This makes it possible to do the convolution only along the x axis. Since the x axis can be converted to the time axis, by the factor of the speed of light, we only need to involve the time variable into the convolution.*

Step 3: *Since the time response is the interesting part, the time distribution of the impulse response is examined. The fastest reflection i.e. the energy reflected at the closest part of the target, x_1, will appear at time t_-. The slowest reflection (at x_2) will in the same way appear at time t_+. Between these two time instants the energy reflection will be uniform due to the plane reflection and the constant square shaped energy distribution.*

Step 4: *The moments t_- and t_+ can, slightly approximated, be calculated through the geometry in Figure 2.6 as*

$$t_- = \frac{2(x_0 - x_-)}{c} = t_0 - \frac{2d}{c\tan\alpha},$$

$$t_+ = \frac{2(x_0 + x_+)}{c} = t_0 + \frac{2d}{c\tan\alpha},$$

where c is the speed of light and t_0 is the mean reflection time for the area. This is equal to the time for a reflection at distance x_0.

Step 5: *The energy reflected at the target is uniformly distributed and can be described by two Heaviside-functions as*

$$h(t) = \frac{\Theta(t_+) - \Theta(t_-)}{t_+ - t_-}$$

$$\textit{where} \quad \Theta(t) = \begin{cases} 1 & \textit{if} \quad t \geq 0 \\ 0 & \textit{if} \quad t < 0 \end{cases}$$

Step 6: *The final pulse shape after reflection can be calculated by convolution*

$$p_{reflected}(t) = (p * h)(t) = \int_0^t p(\tau) \cdot h(t-\tau)\mathrm{d}\tau, \tag{2.8}$$

but since the simulation is discrete this is transformed into the discrete convolution

$$p_{reflected}[t] = (p * h)[t] = \sum_0^t p[\tau] \cdot h[t-\tau]. \tag{2.9}$$

where $p[\tau]$ is the waveform of the pulse sent towards the target.

2.2.2 Bidirectional reflection density function (BRDF)

To describe the reflection properties of the surface the bidirectional reflection density function (BRDF), $\boldsymbol{\rho}$, is used. BRDF describes how the reflected beam spreads into different angles. Figure 2.7 shows an example of a BRDF, where the amplitude is the portion of the energy that is reflected (per steradian) into the specific angle with a source of light where the angle of incidence perpendicular to the surface.

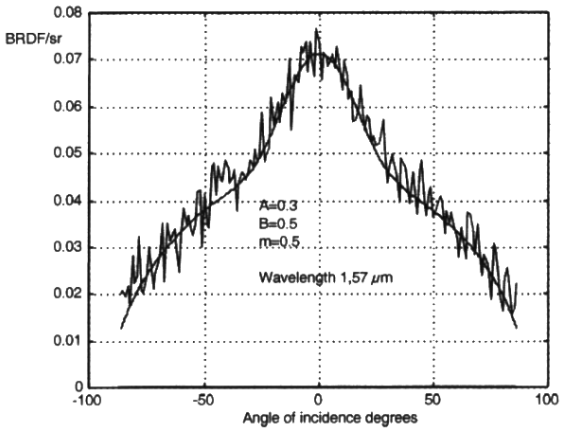

Figure 2.7. An example of a BRDF with the amplitude as a function of the reflected angle when the angle of incidence is parallel to the surface normal. The figure is taken from Steinvall [13].

With some standard assumptions the definition of BRDF, according to Steinvall [12], is

$$\boldsymbol{\rho} = \frac{\text{Surface Radiance}}{\text{Surface Irradiance}} = \frac{\frac{\mathrm{d}P_\mathrm{S}}{\mathrm{d}\Omega_\mathrm{S}}}{P_\mathrm{i}\cos\theta_\mathrm{S}} \approx \frac{\frac{P_\mathrm{S}}{\Omega_\mathrm{S}}}{P_\mathrm{i}\cos\theta_\mathrm{S}},$$

where the variables are depicted in Figure 2.8. The reflected solid angle is given by Ω_S. The incident and scattered light flux is represented by P_i and P_S. Finally, the angles of incidence and scattering are θ_i and θ_S, respectively. In the case of laser radar, the angle of incidence normally coincides with the angle of scattering, i.e. the laser source is positioned at the same place as the receiver. From now on $\theta = \theta_i = \theta_s$ will be used to describe the angle.

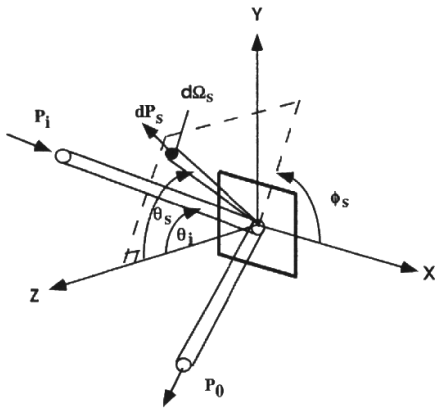

Figure 2.8. Description of the variables used in the BRDF definition. P is a light flux while Θ is an angle. The subscript $_\mathrm{S}$ means the scattering, emitting variable and $_\mathrm{i}$ means the incident variable. Ω_S is the solid angle of scattering. The figure is taken from Steinvall [13].

There are advanced models to calculate the BRDF, which relate it to roughness, surface slope, correlation lengths, refractive index etc., but many of them tend to get too complicated. Some interesting simplified models have been published, and Steinvall [13] presents one of them as

$$\boldsymbol{\rho} = \boldsymbol{\rho}_{\text{spec}} + \boldsymbol{\rho}_{\text{diff}} = \frac{A}{\cos^6(\theta)} e^{-\frac{\tan^2(\theta)}{s^2}} + B\cos^m(\theta) \tag{2.10}$$

where A and B are constants describing the relation between the specular and diffuse reflection. Specular reflection is the straight reflection, as described in Figure 2.4. It can be recognized as the peak in the middle of Figure 2.7. The diffuse reflection supports the base reflection below the peak in the middle and covers reflection into almost any angle. The momentary slope is represented by s, and m is a parameter describing the diffuse surface. The angles of incidence and reflection are equal, θ.

The BRDF is measured per steradian [sr^{-1}], which is defined as the solid angle which, having its vertex at the center of the sphere, cuts off an area equal to the square of its radius. This means, 1 steradian has a projected area of 4 square meters at a distance of 2 meters.

2.2.3 Speckle

As described in [6], speckle is a phenomena which arises from the reflection of coherent illumination from a diffuse surface. The diffuse surface creates an array of scatterers that is independent of each other, randomly phased and independent of time. When these interfere, dark and bright spots, called speckle cells, seem to appear on the surface. If the detected area of the receiver is larger than one speckle cell, averaging will occur between the cells inside the detected area of the receiver. An example of speckle modulation of the light intensity across an area is found in Figure 2.9.

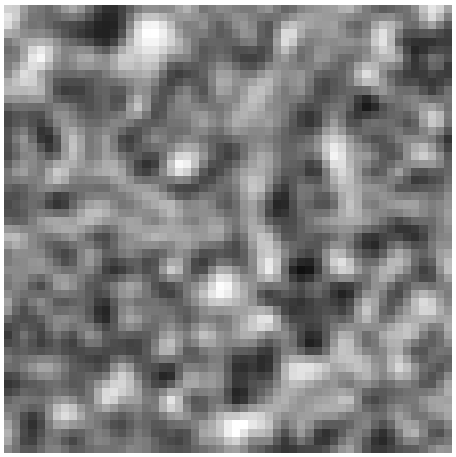

Figure 2.9. One pixel with speckle cells of a specific cell size and random values determined by the speckle pdf, equation (2.11). White represents a higher intensity than black.

To determine the diameter of the speckle cells D_{sp}, an approximation is introduced in Steinvall [14], and is defined as

$$D_{\text{sp}} = \frac{\lambda}{\phi},$$

where λ is the wavelength and ϕ is the beam divergence of the laser. The value of the intensity for each speckle cell can be randomly determined by the probability density function (pdf)

$$P_{\text{dir,M}}(S) = \frac{\left(\frac{M}{S_{\text{av}}}\right)^M \cdot S^{M-1} \cdot e^{-M\frac{S}{S_{\text{av}}}}}{\Gamma(M)}, \tag{2.11}$$

where $M = D_{\text{rec}}/D_{\text{sp}}$ and D_{rec} is the aperture diameter of the receiver, i.e. the diameter of the optical input at the receiver. From this discussion, M is the number of speckle cells that are seen by the receiver (measured in one dimension). The value of the detected signal is named S, and its time average S_{av}.

2.3 Atmospheric effects

The atmosphere will affect the signal in several ways. First of all, it will broaden the beam, depending on, for instance, turbulence and beam divergence. Secondary, it will cause random intensity fluctuations, called scintillations. Finally, it will cause attenuation, and the beam will be weaker as the range increases. Actually, the turbulence makes the light go other ways than the straight way, because when the air particles move around they randomly change the refractive index of the air. Since that would be very complicated to simulate, those three mentioned disturbances give a good approximation. Another thing that affects the beam is *backscattering*, which occurs when the laser source and the receiver are placed close to each other. The particles in the air will reflect parts of the beam energy directly into the receiver before the main part has reached the target, and the receiver will detect this at much higher level than the target reflection. This is however most often treated directly in the receiver, which does not detect the backscattered energy. Therefore, backscatter will be ignored in this report and the simulation program. To read more about this, see *IR/EO Handbook* [6].

As a measurement of the strength of the turbulence, C_{n}^2 is used, with the odd unit $m^{-2/3}$. It varies slowly over the day and reaches maximum at about noon, while the lowest values occur from sunset until dawn. This derives from the temperature gradient and wind velocity, which usually are low at night. Close to the ground, the turbulence is stronger than high up in the atmosphere.

2.3.1 Beam broadening

Due to the turbulence the beam will spread out in the medium. In the following equations, $k = \frac{2\pi}{\lambda}$ is the wave number. According to Steinvall [12], the beam broadening follows

$$w_{\text{spread}} = w \cdot \sqrt{1 + 1.624 \cdot (\sigma^2_{\text{Rytov}})^{6/5} \cdot \Lambda_1}, \tag{2.12}$$

$$\text{where} \quad \sigma^2_{\text{Rytov}} = 1.23 \cdot C_{\text{n}}^2 \cdot k^{7/6} \cdot R^{11/6}, \quad \Lambda_1 = \frac{\lambda R}{\pi w^2}.$$

2.3.2 Intensity fluctuations

As in speckle calculations the spatial area of interest (the beam foot print) is divided into turbulence cells. In each turbulence cell the intensity of the beam energy is randomly determined by a given pdf, in the same way as in the speckle case. Note that the cell sizes of turbulence and speckle does not necessarily correspond. An example of turbulence fluctuations is shown in Figure 2.10.

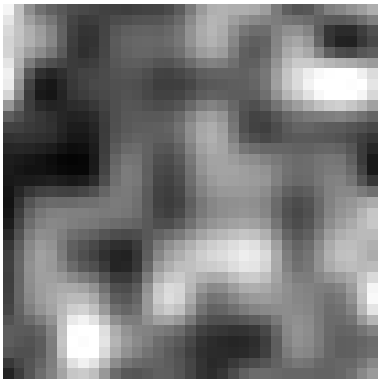

Figure 2.10. One pixel with turbulence cells of a specific cell size and random values determined by the turbulence pdf, equation (2.13). White represents a higher intensity than black.

The pdf of the intensity fluctuations [14] is described by

$$P_{\text{turb}} = \frac{1}{S \cdot \sqrt{2\pi\sigma^2_{\ln I}}} \exp\left(-\frac{\left(\ln(\frac{S}{S_{\text{av}}}) + \frac{1}{2}\sigma^2_{\ln I}\right)^2}{2\sigma^2_{\ln I}} \right). \tag{2.13}$$

The time compensated value according to log-intensity variance, $\sigma^2_{\ln I}$, is given by

$$\sigma^2_{\ln I} = \ln(1+\sigma^2_I) = \ln(1+\sigma^2_{\text{target}}),$$

where σ^2_{target} is the effective turbulence fluctuations after target averaging and determined by

$$\sigma^2_{\text{target}} = \gamma_{\text{target}} \cdot \sigma^2_{\text{sat,point}}. \tag{2.14}$$

The first factor in equation (2.14) is an averaging term described by

$$\gamma_{\text{target}} = \left(\frac{\rho_{\text{l}}}{r_{\text{eff}}}\right)^{7/3},$$

while the second term is the σ^2_{point} saturated at 1.3 according to

$$\sigma^2_{\text{sat,point}} = \frac{1.3 \cdot \sigma^2_{\text{point}}}{1+\sigma^2_{\text{point}}}.$$

As a first approximation, double path turbulence can be modeled by

$$\sigma^2_{\text{point}} = 1.23 \cdot C^2_{\text{n}} \cdot k^{7/6} \cdot (2R)^{11/6},$$

where C^2_{n} is the turbulence constant and $k = 2\pi/\lambda$ is the wave number. The target range is represented by R.

The radius of the effective averaging spot is determined by

$$r_{\text{eff}} = \min(r_{\text{target}},\ w,\ \frac{\vartheta_{\text{fov}}}{2}R), \tag{2.15}$$

where r_{target} is the geometric radius of the target, w is the laser beam radius at target and $\frac{\vartheta_{\text{fov}}}{2}R$ is the target radius seen by the receiver. This is valid since ϑ_{fov} is the *field of view*, i.e. the one dimensional angle of sight through the receiver according to Figure 2.11, and the ϑ_{fov} always is small.

To determine the (one dimensional) radius of one turbulence cell, ρ_{l}, the following relation from Steinvall [14] is used:

$$\rho_{\text{l}} = \frac{\sqrt{\frac{R}{k}}}{\sqrt{1+\frac{R}{k\rho_0^2}}}, \tag{2.16}$$

$$\text{where} \quad \rho_0 = \rho_{0,\text{p}} \cdot \left(\frac{\left(1-\frac{R}{f}\right)^2 + \left(\frac{R}{z_{\text{B}}}\right)^2 (1+\frac{\delta^2}{3}) \cdot \frac{1}{1+\delta^2}}{1-\frac{13R}{3f}+\frac{11}{3}\left(\frac{R}{f}\right)^2 + \frac{1}{3}\left(\frac{R}{z_{\text{B}}}\right)^2 + \frac{1}{3}\left(\frac{R}{f}\right)^2 \cdot \frac{1+\frac{\delta^2}{4}}{1+\delta^2}} \right)^{1/2},$$

$$\rho_{0,\text{p}} = (1.46 \cdot k^2 C_{\text{n}}^2 R)^{-3/5},$$

$$z_{\text{B}} = \left(\frac{kw_0}{2}\right) \cdot \left(\frac{1}{\rho_{0,\text{s}}^2} + \frac{1}{4w_0^2}\right)^{-1/2},$$

$$\rho_{0,s} = (0.5 \cdot k^2 C_{\text{n}}^2 R)^{-3/5},$$

$$f = \frac{-w_0}{\tan(\frac{\phi}{2}) - \tan(\frac{\lambda}{2\pi w_0})}$$

$$\text{and} \quad \delta = \frac{2w_0}{\rho_{0,\text{p}}},$$

where f is the receiver focal length, ϕ is the beam divergence and $\rho_{0,(\text{p,s})}$ is the transverse coherence length for a spherical (s) or plane (p) wave.

2.3.3 Aerosol attenuation

The particles in the air absorb and reflect the light and cause attenuation of the beam. The attenuation factor can, as in Steinvall [14], be described by

$$\Psi_{\text{attenuation}} = e^{-2R \cdot \boldsymbol{\sigma}_{\text{aer}}}, \tag{2.17}$$

where R is the target range and the aerosol attenuation

$$\boldsymbol{\sigma}_{\text{aer}} = \frac{3.91}{V_{\text{M}}}\left(\frac{\lambda}{0.55}\right)^{-q}. \tag{2.18}$$

The wavelength is λ and the visibility distance is V_{M}. In Steinvall [14], the variable q is described as

$$q = \begin{cases} 1.6 & \text{if} \quad V_{\text{M}} > 50 \text{ km}, \\ 1.3 & \text{if} \quad 50 \text{ km} > V_{\text{M}} > 6 \text{ km}, \\ 0.585 \cdot V_{\text{M}}^{0.33} & \text{if} \quad 6 \text{ km} > V_{\text{M}}. \end{cases} \tag{2.19}$$

Equation (2.19) is valid only for wavelengths of about 0.5-2 μm, but since this is normal for a laser radar system, this is a good approximation.

2.4 Receiver properties

The receiver is by no means ideal and introduces noise both in the detection and in the amplifying stage. Der et al. [4] present a way to simulate this noise.

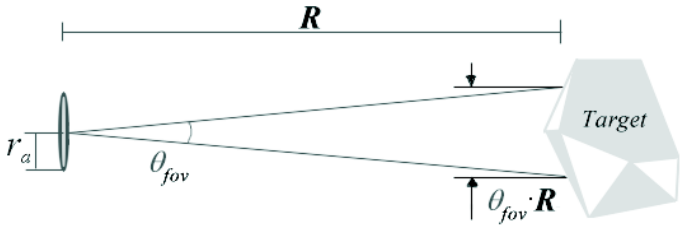

Figure 2.11. The receiver setup and its assignments.

The factors involved in the noise are so many that they deserve separate explanations. They are all listed in Table 2.1 and some of them are related to Figure 2.11.

Noise affecting receiver parameters		
r_a	[m]	Aperture radius
B	[MHz]	Bandwidth
$\Delta\lambda$	[μm]	Optical filter bandwidth
e_c	[C]	Elementary charge ($1.602{\cdot}10^{-19}$)
f	[m]	Focal length
F	[-]	Excess noise factor
h_sun	[W/m^2/μm]	Sun spectral irradiance, see section 2.4.1
I_ampl	[A]	Amplifier current
I_b	[A]	Background illumination current
I_db	[A]	Dark bulk current
I_ds	[A]	Dark surface current
I_s	[A]	Signal current
M	[-]	Detector internal gain
$\Re$	[A/W]	Responsivity
ϱ	[sr^{-1}]	Mean background reflection
T_r	[-]	Optical Transmission
ϑ_fov	[mrad]	Instantaneous field of view

Table 2.1. The receiver parameters affecting the receiver noise and their explanations.

Putting these parameters together gives us the noise equivalent power (NEP) from the detector as

$$\mathrm{NEP}_\mathrm{detector} = \frac{(2e_\mathrm{c}B\cdot(I_\mathrm{ds}+(I_\mathrm{db}+I_\mathrm{b}+I_\mathrm{s})M^2F))^{1/2}}{\Re}. \tag{2.20}$$

Most of these parameters have to be known explicitly though two of the currents can be calculated:

$$I_\mathrm{s} = \Re P_\mathrm{turbulence},$$

$$\text{and} \quad I_\mathrm{b} = \Re P_\mathrm{b} = \Re\varrho\, h_\mathrm{sun} T_\mathrm{r}\cdot\pi r_\mathrm{a}^2\cdot\sin^2\left(\frac{\vartheta_\mathrm{fov}}{2}\right)\Delta\lambda, \tag{2.21}$$

where the variables are described in Table 2.1.

To be able to simulate the amplifier noise, the construction of it has to be known. This is normally not the case, and therefore the assumption of some construction layout has to be made and as an example of amplifier, a RC filtered amplifier is used, suggested by Der et al. [4]. This amplifier gives a noise level of

$$\mathrm{NEP}_{\mathrm{ampl}} = \sqrt{\frac{4kTBN}{R_{\mathrm{L}}\Re^2}},$$

where k is Boltzmann's constant, T is the temperature in degrees Kelvin, N is the noise factor for the electronics and R_{L} is the load resistor calculated from

$$R_{\mathrm{L}} = \frac{1}{2\pi BC},$$

where C is the capacitance of the detector. The $\mathrm{NEP}_{\mathrm{ampl}}$ and $\mathrm{NEP}_{\mathrm{det}}$ is combined together into a $\mathrm{NEP}_{\mathrm{total}}$ which is interpreted as the standard deviation for the Gaussian distribution of the additive noise

$$\mathrm{NEP}_{\mathrm{total}} = \sqrt{\mathrm{NEP}^2_{\mathrm{detector}} + \mathrm{NEP}^2_{\mathrm{ampl}}} \tag{2.22}$$

2.4.1 Background solar irradiance

The background solar irradiance is depending on many factors. The simulations are therefore using a simple, but not too incorrect, approximation.

First of all, the expression h_{sun}, introduced in equation (2.21) and Table 2.1, is only an approximation. In fact, to consider the reality, the position of the sun or the moon, the weather right at the moment, the season, the time of the day, the position and direction of the receiver and many more parameters have to be considered. To consider almost everything of this there are simulation programs such as MODTRAN^{TM} and HITRAN^{TM}. Figure 2.12 shows one example of the result from a simulation made by MODTRAN^{TM}. The upper curve shows the illumination outside the atmosphere and the lower curve shows the same but inside the atmosphere. Note that some wavelengths are almost totally absorbed by the atmosphere.

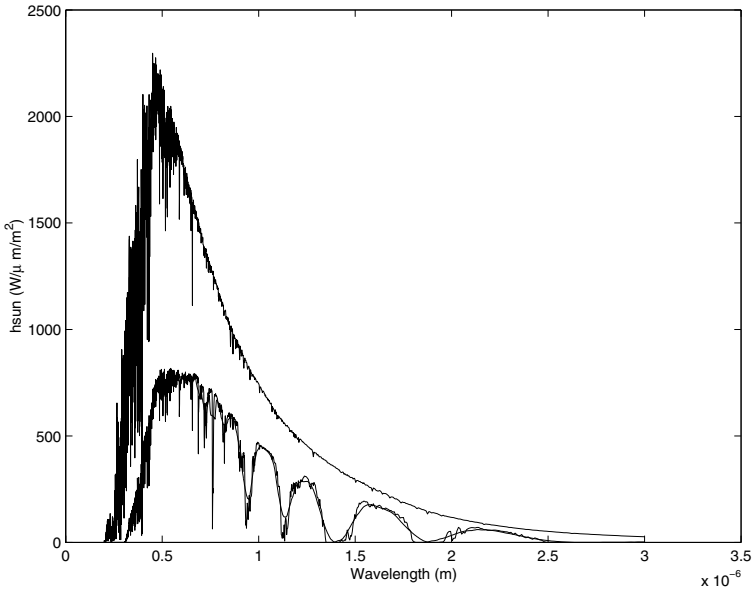

Figure 2.12. The background solar irradiance. The upper curve is outside the atmosphere and the lower curve at earth level inside the atmosphere.

To simplify this part, a curve (in fact the curve in Figure 2.12) is used as a template and its amplitude is scaled for different conditions. The scale factor is decided from Table 6-9 on page 70 in the Electro-Optical Handbook [2] and also shown in Table 2.2. The rightmost column is normalized to direct sunlight and is used as the scale factor in the implementation. This means that Figure 2.12 represents the maximum solar irradiance and that the sky condition alternatives only can make the light intensity lower.

Sky conditions	**Approx. Levels of Illuminance - lux [lm/m^2]**	**Normalized illuminance**
Direct sunlight	$1 - 1.3 \cdot 10^5$	1
Full daylight	$1 - 2 \cdot 10^4$	0.14
Overcast day	10^3	$9.1 \cdot 10^{-3}$
Very dark day	10^2	$9.1 \cdot 10^{-4}$
Twilight	10	$9.1 \cdot 10^{-5}$
Deep twilight	1	$9.1 \cdot 10^{-6}$
Full moon	10^{-1}	$9.1 \cdot 10^{-7}$
Quarter moon	10^{-2}	$9.1 \cdot 10^{-8}$
Moonless, clear night sky	10^{-3}	$9.1 \cdot 10^{-9}$
Moonless, overcast night sky	10^{-4}	$9.1 \cdot 10^{-10}$

Table 2.2. Illuminance scale factors. The rightmost column is a normalized version of the middle column. The data in the table are taken from Burle [2].

2.5 3-D laser radar systems and the radar equation

2.5.1 System setup

There are two main categories of 3-D laser radar systems.

1. The first type uses a scanning technique where the target is scanned with laser pulses with only one receiver sensor necessary. The target is therefore separated into an array of laser pulses.

2. The second type uses a camera technique where only one wide laser pulse includes all parts of the target while instead the receiver is divided into an array of small detectors, each only detecting a part of the target.

Both these types end up in the same theory mostly due to equation (2.15) on page 17. The effective radius is the smallest of the beam radius, the receiver radius at target and the smallest physical radius of the target. In the first case above, the beam radius is the smallest but in the second case the receiver area at target is the smallest one. To get a descent resolution in the result, about the same radius is wanted in both cases. Therefore the two cases end up in almost the same calculations and the same simulation tool can be used.

2.5.2 Transformed radar equation

The original radar equation, as stated in Skolnik [11], can according to Steinvall [13] be transformed into a laser radar equation:

$$P_{\mathrm{r}} = \frac{P_{\mathrm{T}} G_{\mathrm{T}}}{4\pi R^2} \cdot \frac{\varsigma_{\mathrm{cs}}}{4\pi R^2} \cdot A_{\mathrm{a}}, \tag{2.23}$$

where the transmitted(/received) power is $P_{\mathrm{T(/r)}}$, G_{T} is the antenna gain, w_{T} is the transmitter beamwidth, ς_{cs} is the effective target cross section, R is the target range, r_{a} is the receiver aperture radius and A_{a} its area, λ is the wavelength and η are inefficiencies and disturbances caused by the atmosphere and the receiver system.

Since the system is known, we assume a radial symmetric receiver aperture and introduce the inefficiency in atmosphere, η_{atm}, and in the system, η_{syst};

$$P_{\mathrm{r}} = \frac{P_{\mathrm{T}} G_{\mathrm{T}}}{4\pi R^2} \cdot \frac{\varsigma_{\mathrm{cs}}}{4\pi R^2} \cdot \pi r_{\mathrm{a}}^2 \cdot \eta_{\mathrm{atm}} \eta_{\mathrm{syst}}. \tag{2.24}$$

Since $G_{\mathrm{T}} = 4\pi / w_{\mathrm{T}}^2$, A_{Ta} is the target area and ϱ_{refl} is the target reflectance, the equation can be transformed into

$$P_{\mathrm{r}} = \eta_{\mathrm{syst}} \cdot \underbrace{\frac{4P_{\mathrm{T}}}{\pi w_{\mathrm{T}}^2 R^2}}_{\substack{\text{Illuminance} \\ \mathrm{W/m^2}}} \cdot \varrho_{\mathrm{refl}} A_{\mathrm{Ta}} \cdot \underbrace{\frac{\pi r_{\mathrm{a}}^2}{\Omega_{\mathrm{Ta}} R^2}}_{\substack{\text{Fraction} \\ \text{scattered} \\ \text{into} \\ \text{receiver}}} \cdot T_{\mathrm{atm}}^2, \tag{2.25}$$

where T_{atm} is the two-way atmospheric loss, and Ω_{Ta} the solid angle into which the target reflection scatters. For a well resolved target, equation (2.25) can be reduced to

$$P_r = \eta_{\mathrm{syst}} \cdot P_{\mathrm{T}} \cdot \varrho_{\mathrm{refl}} \cdot \frac{\pi r_{\mathrm{a}}^2}{\Omega_{\mathrm{Ta}} R^2} \cdot T_{\mathrm{atm}}^2, \tag{2.26}$$

and to finally turn it into a laser radar equation we change it to

$$P_{\mathrm{r}} = \eta_{\mathrm{syst}} \cdot \frac{E_{\mathrm{p}}}{2\tau} \cdot \underbrace{\boldsymbol{\rho} \cdot \frac{\pi r_{\mathrm{a}}^2}{R^2}}_{\mathrm{BRDF}} \cdot e^{-2\boldsymbol{\sigma}_{\mathrm{aer}} R}. \tag{2.27}$$

Identification of equation (2.27), which also appears in Der et al. [4], makes some things clear. The first factor, η_{syst}, is the system efficiency. The second factor, $E_{\mathrm{p}}/(2\tau)$, is the peak power factor of the signal. It is followed by the BRDF which consist of two factors where the first factor, $\boldsymbol{\rho}$, is the BRDF per steradian and the second factor is the number of steradians the receiver aperture covers as seen from the target reflecting the beam. The last factor, $e^{-2\boldsymbol{\sigma}_{\mathrm{aer}} R}$, is the aerosol attenuation caused by aerosol particles in the atmosphere.

2.6 Conclusions

This section contains a brief listing of the equations and tables that is used in the simulation further in the report.

- Laser source
  - Spatial distribution - eq. (2.2) and eq. (2.4)
  - Time distribution - eq. (2.1)
- Target
  - Geometric structure - eq. (2.9)
  - BRDF - eq. (2.10)
  - Speckle - eq. (2.11)
- Atmosphere
  - Beam broadening - eq. (2.12)
  - Intensity fluctuations - eq. (2.13) and eq. (2.16)
  - Aerosol attenuation - eq. (2.17)
  - Background solar irradance - table (2.2)
- Receiver
  - Receiver parameters - table (2.1)
  - Amplifier and receiver noise - eq. (2.22)
- General
  - System setup factors - eq. (2.27)

3 Simulation ideas

3.1 Inputs

As input there is a CAD description of the target and its surroundings. It is grabbed as a DXF file from a 3-D graphics program (for instance AutoCad), exported into MATLAB and converted into patches, see Figure 3.1 and [9].

The information about a target required to perform a simulation is as follows: the positions of the vertices (corners), the faces (planes connecting the vertices), the BRDF (see section 2.2.2) of the faces and the angle of view expressed as azimuth and elevation, see [9].

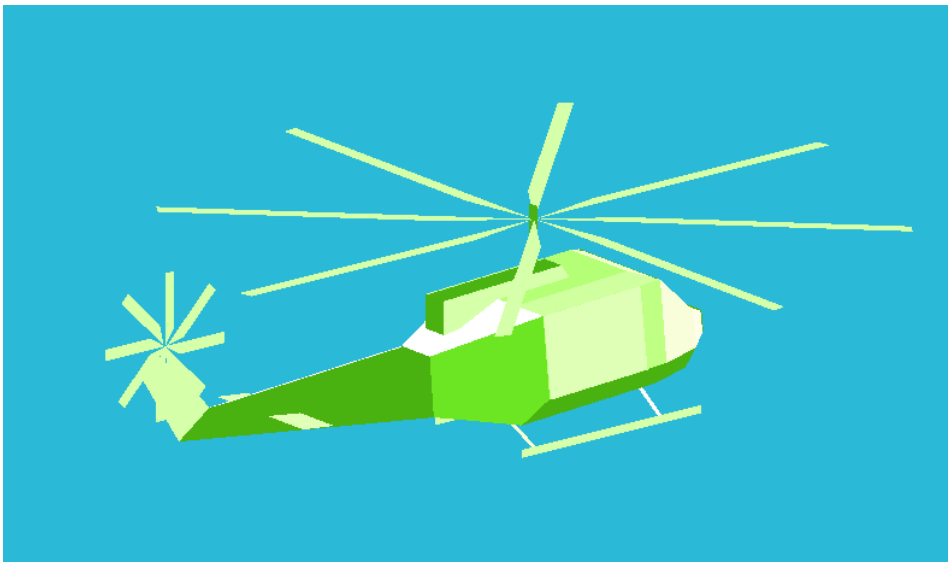

Figure 3.1. A target example described as patches in MATLAB.

3.2 Simulation steps

The simulation consists of several steps. The central structure of the simulation has been derived from Der et al. [4] and Der et al. [5]: (Consequently a pixel is one simulation spot (one laser shot), made up by a number of subareas. A subarea is the smallest division used in the simulation)

1. Define the laser, target, atmosphere and receiver properties.

2. Project the 3-D view of the target into a distance image (Figure 3.2) with information about the normal vector of the surface in each pixel. The resolution is not too good (0.1-0.5 m), since each pixel represents one laser beam or one receiver cell (see section 2.5).

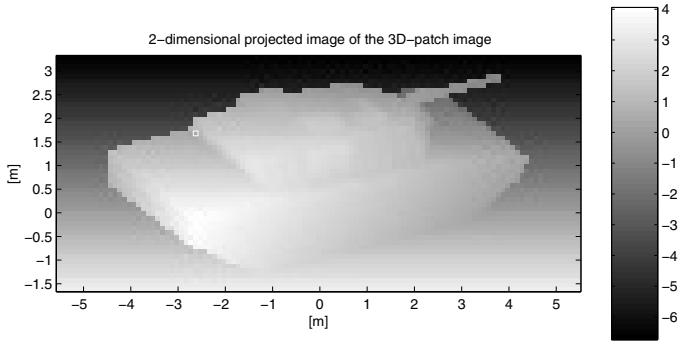

Figure 3.2. A projected image from a 3-D patch description. The colorbar (right) shows the distance to each pixel, with origo as defined in the original 3-D patch description.

3. Divide every pixel into a number of subareas and create as many as possible. Determine the normal vector and depth in each subarea. Each subarea is represented as a plane surface with the properties of its center spot, see Figure 3.3.

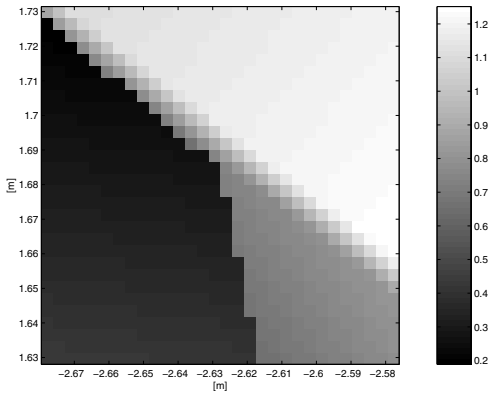

Figure 3.3. One pixel (indicated by the white rectangle in Figure 3.2) divided into 30x30 subareas. The colorbar (right) shows the distance to each pixel, same scale as Figure 3.2.

4. Consider one laser beam area (pixel) at a time. Divide the laser pulse power into the subareas, see upper left corner of Figure 3.4.

5. Keep the subarea division and set the speckle and the turbulence fluctuation cell size and calculate their pdf. Get random values for these in each subarea, see the right side of Figure 3.4. Observe the difference in cell size that usually occurs, since the cell sizes depend on different factors. The bottom left part of the figure, shows the resulting laser beam, after both speckle and turbulence affection.

6. Let each subarea of the laser beam be reflected on the target. The target is, as mentioned, in each subarea considered to be plane and the reflection follows the rules from section 2.2.1. As a result, one individually reflected pulse in each subarea is given.

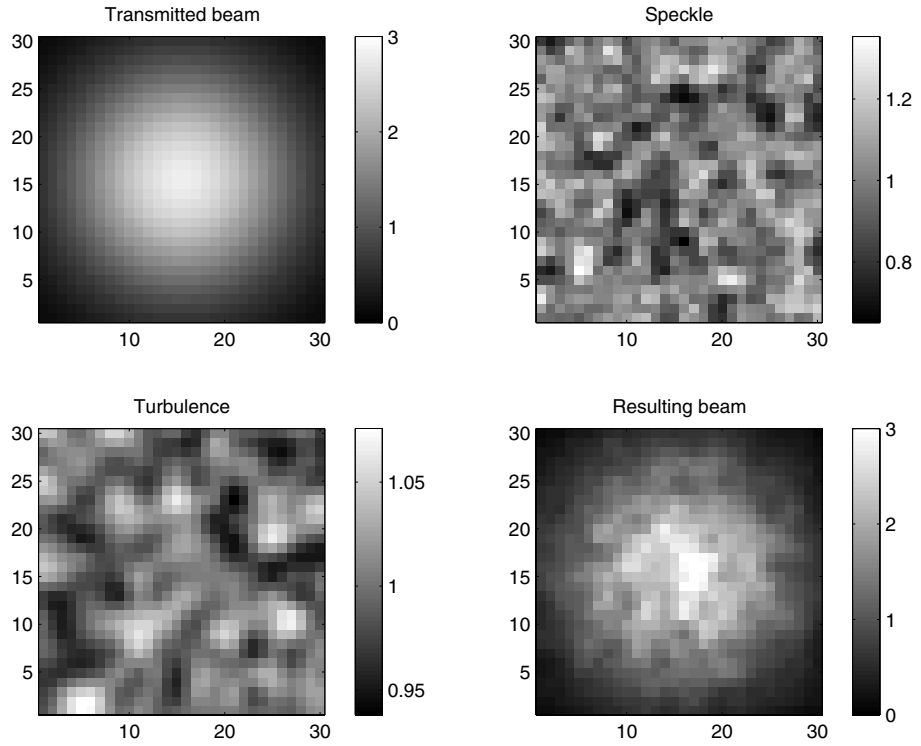

Figure 3.4. The irradiance distribution of a laser beam. Top left is the original beam, top right is the speckle pattern, bottom left is the effect of turbulence and bottom right is the total beam after speckle and turbulence disturbances.

7. For each time step, calculate the resulting laser pulse energy in each subarea and add up all those within the same original pixel into a wave representing the reflection from one single laser beam.

8. Let the receiver noise disturb the resulting waveform (Figure 3.5).

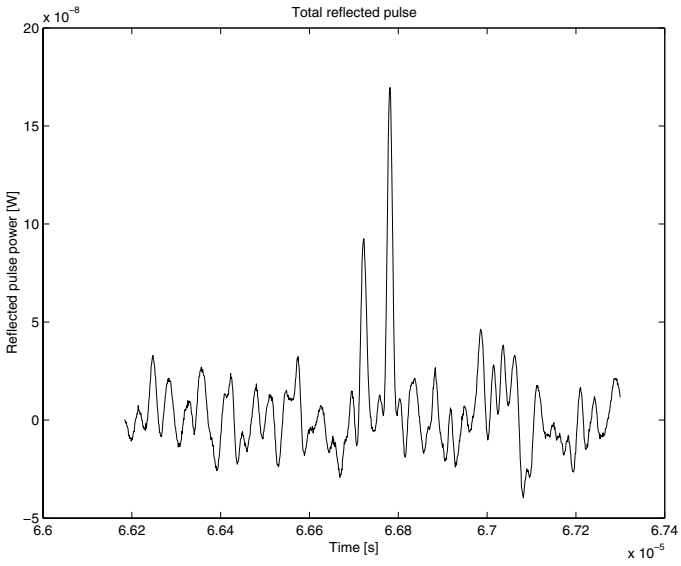

Figure 3.5. The final, reflected and noise affected, 3-D laser radar waveform in the chosen pixel.

4 Validation

4.1 Instrumentation

Since there were no existing **3-D** laser radar system available at the department, a simplified manual method to simulate the 3-D scanning technique had to be used. The existing instrument was a single shot laser radar system, an *Optech Rangefinder 501SX* [10], see the specifications in Table 4.1 below. The laser radar system was placed on the fourth floor and the laser pointed at a target placed on the ground.

Property	**Value**
Wavelength	904 nm
$T_{1/2}$	15 ns
Beam Divergence	2.5 mrad
Pulse Energy	0.0025 mJ
Focusing Range	0.5 km
Receiver Aperture Radius	0.075 m

Table 4.1. Specification of the laser radar system.

The laser radar system amplifies and filters the signal automatically, without the possibility to extract the unprocessed signal. To display the result, a digital oscilloscope, *LeCroy LC534A*, was used. The waveform was stored directly by the oscilloscope on diskette in MATLAB format. The time resolution was limited to a minimum of 2 ns and the amplitude resolution was discrete.

4.2 Environment

The atmosphere was the most difficult part to get exact values from. The approximations and assumptions are listed in Table 4.2.

Property	**Value**
Visibility	5 km
Attenuation	$4.2{\cdot}10^{-4}\ m^{-1}$
Solar spectral irradiance	410 $\mathrm{W/m^2/\mu m}$
Turbulence constant C_n^2	$1.02{\cdot}10^{-15}\ \mathrm{m^{-2/3}}$

Table 4.2. The atmosphere environment during the validation test.

4.3 Target

The target used for validation was a military vehicle standing in the backyard of FOI. The shape of the target was imported into the simulation tool manually, see Figure 4.2. A picture of the target is shown in Figure 4.1 below. The average distance to the target was 110 m. Figure 4.2 shows the approximation of the vehicle imported into MATLAB.

Figure 4.1. A photo of the vehicle used for validation.

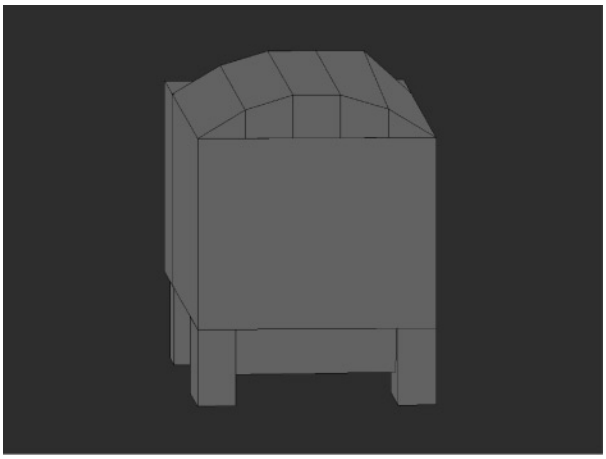

Figure 4.2. The MATLAB representation of the vehicle used for validation.

4.4 Results

To validate the toolbox, the properties of the environment, the target, the laser source and the receiver were estimated and the reflected waveform were simulated in every pixel of the image. To compare the result, the waveform and the distance image were used. The simulated waveform itself turned out to be hard to compare to the corresponding measured waveform due to the filtering and amplification inside the laser radar equipment, but the distance images were possible to compare.

4.4.1 Waveform validation

The signal on the oscilloscope was, as mentioned, not completely corresponding to the simulated one, mostly due to the post filtering performed by the laser radar. Though, to compare the results, two examples of waveforms are shown in Figure 4.3. Those waveforms are taken from the upper left part of the vehicle, see Figure 4.1.

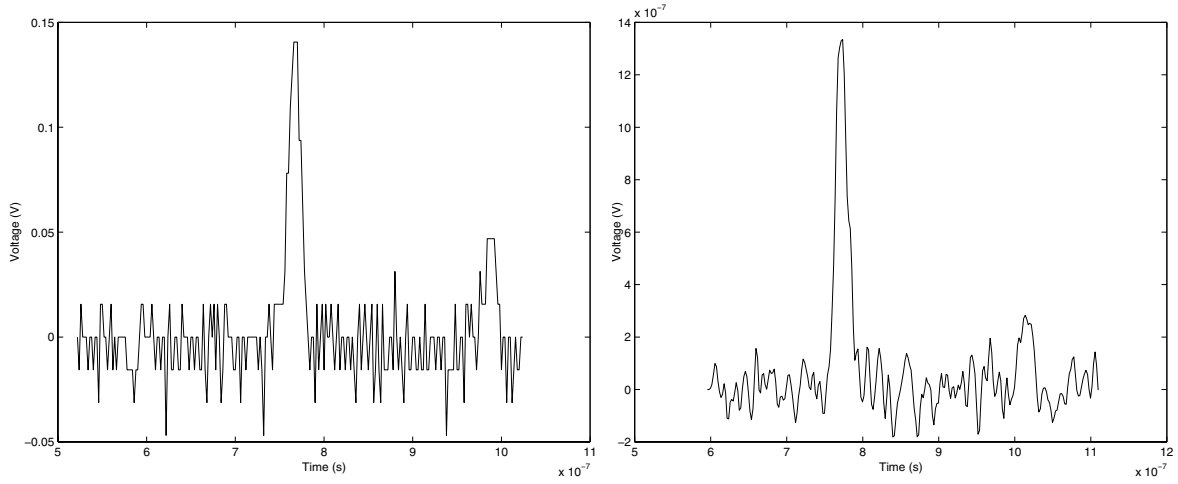

Figure 4.3. The measured data to the left and the simulated data to the right. The waveform is taken from the upper left edge of the vehicle.

The first, larger, pulse comes from the reflection against the vehicle roof, and the last pulse is the reflection against the ground behind the vehicle. The left waveform comes from the measured data, and the simulated waveform is on the right. The left, measured, data is more discretizised than the simulated data, but apart from this they are almost identical. The power scaling is also different, though this comes from the internal amplification, that is normally external and does not belong to the laser radar. This is not treated by the simulation program since this is a special case.

4.4.2 Distance image validation

To validate the distance image, waveforms were simulated in several positions across the target, approximately corresponding to the positions measured with the laser radar equipment. This procedure was followed by peak detection algorithms to detect the distance to the target in every pixel. Undetectable peaks result in drop-outs which are represented by black pixels in the image. For full explanation of the term *drop-out*, see section 5.5 on page 35.

In Figure 4.4, the result is shown. To the left is the perfect distance image, in the middle is the simulated distance image and to the right is the measured distance image. The drop-outs appear on the most oblique areas where a smaller amount of energy is reflected back to the receiver. The scale differences between the measured data and simulated data are due to the manual scanning of the laser beam, which did not follow a perfectly quadratic grid.

4.4.3 Conclusions

In conclusion, the validation of the toolbox did not verify the algorithms with high accuracy. Though, the result seems to be accurate enough, and since the algorithms have been verified in other tests and are generally accepted amongst laser radar scientists, it is reasonable to assume that the toolbox is valid.

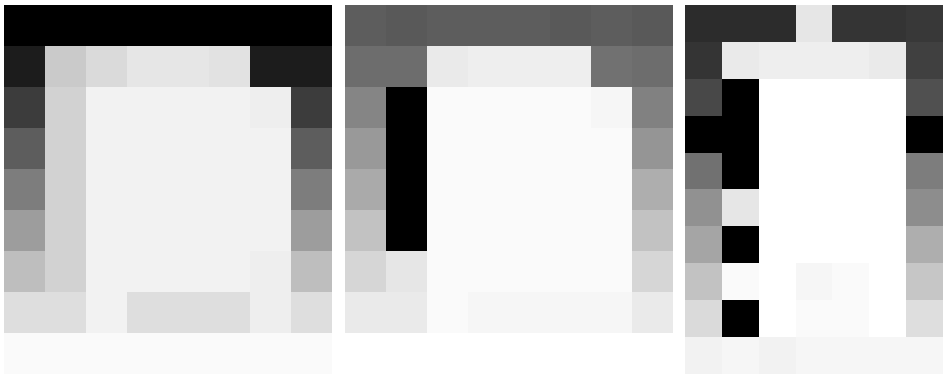

Figure 4.4. The distance images where the intensity represents the distance to the target. From left to right we have the correct distance, the simulated distance and finally the measured distance. The black spots are drop-outs, where the signal peak is to low to be detected. White areas are close and dark areas are far away.

5 Target recognition

The focus in this section will lie on recognizing the most simple waveforms, i.e. flat surface reflection, oblique surface reflection and step reflection. The first part of this section describes the typical characteristics of a perfectly reflected pulse at different surface slopes. The following sections will treat the pulse detection, the classification, the noise aspect, the robustness of the decisions and results of the experiments.

5.1 Perfect reflection

To determine the normal behavior of a plane reflection at a target of different surface slopes a simulation was made at a target specially made for this purpose. The target consisted of a simple wall with discretely increasing slope, from one edge to the other, see Figure 5.1. A scanning laser radar technique was used and as result, eight pulses were given, each representing a different slope. They are all given in Figure 5.2. At first, no noise was applied to the pulses, just to see if it was possible to determine the surface slope from perfect signals. The figure shows that different slopes give different widths of the reflected pulses. The leftmost surface part of Figure 5.1 correspond to the closest waveform in Figure 5.2. This is the effect that will be used to detect different slopes. The perfect signals in Figure 5.2 are used as templates that are compared to the reflected pulse from an unknown target. A suggestion of target recognition using templates is described in section 5.2.

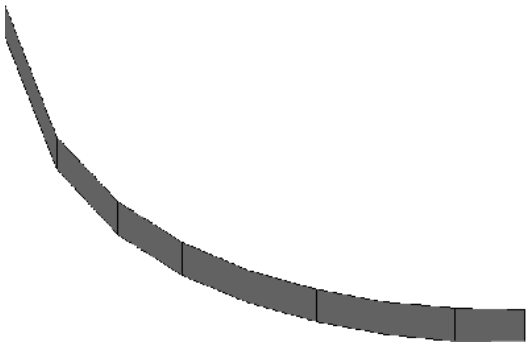

Figure 5.1. The target used for tests of the reflection for different slopes.

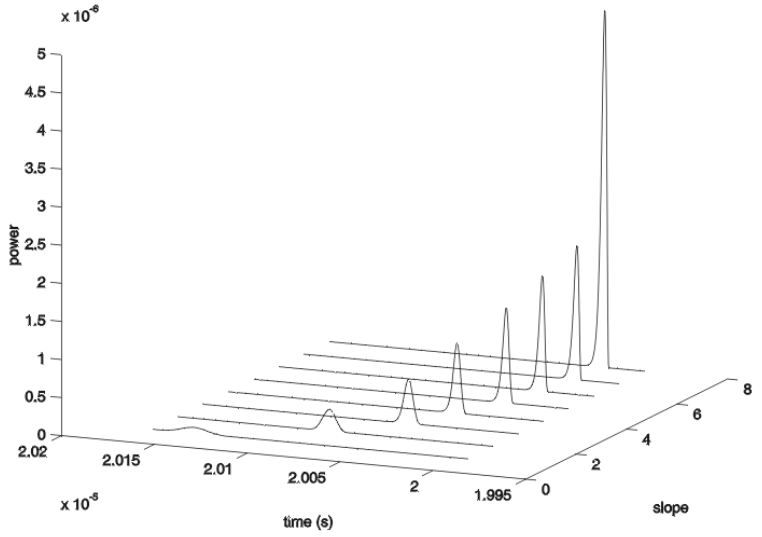

Figure 5.2. The reflected pulse at the eight different slopes. The widest pulse has been reflected at the most sloping surface, i.e. the closest waveform has been reflected on the left part of the wall in Figure 5.1.

5.2 Error calculation method

To identify different sloping surfaces the noise-less perfectly reflected signal for those template surfaces can be compared to some unknown surface reflections. To compare the pulses, this method uses the sum of the square of the errors. The algorithm looks at a length of the signal as large as the length of the perfect pulse, with the maxima fitting together. In Figure 5.3 the test pairs of one perfect pulse and one unknown are seen. Each row treats one test signal, and each column treats one template pulse. The correct corresponding pairs are found in the diagonal (from upper left corner to lower right corner).

The error estimation algorithm is described by

$$E = \sum_{t_0}^{t_\mathrm{f}} \frac{(p_\mathrm{perfect}[t] - p_\mathrm{test}[t])^2}{t_\mathrm{f} - t_0}, \tag{5.1}$$

where $p[t]$ is the pulses and E square error. The start and end time is decided by synchronizing the maxima of the signals and letting the template pulse draw the limits of this error calculation. In Figure 5.3, this distance can be seen since every template pulse is of sufficient length while the test pulses are being stretched during tests against the different templates. The division in equation (5.1) is made as a compensation for the different lengths of the calculations, to calculate the error value per time unit.

The classification method converts all the error values of different template comparisons to numbers between one and zero, where the value *one* is given to the signal with the lowest error i.e. the most probable guess, and the other signal values fall on the scale to zero. Values close to one are also probable and should be considered as possible answers. To get the current angle estimation, these probabilities are weighted together and from the template angles, the estimated angle can be calculated.

Tests with perfect signals resulted in no error at all and every pulse was classified correctly. With noise, the classification was worse, but good enough. Though, to be able to detect the signal peaks correctly, a simple smoothing has to be done. However, the highest sloping surface

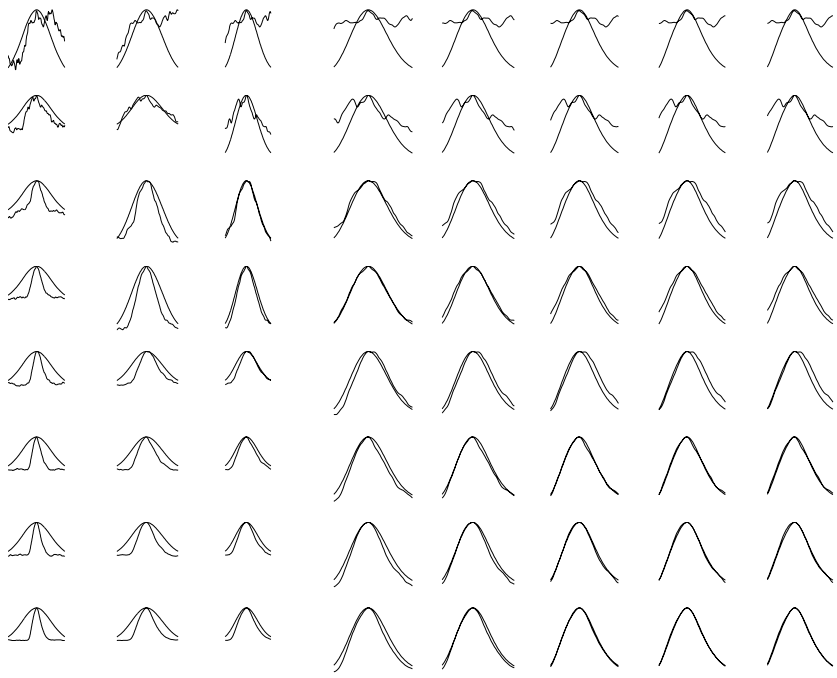

Figure 5.3. The test pairs with eight pulses as input (the rows) and eight template pulses (the columns). The resulting classification for this set of data can be seen in Figure 5.4.

is still a problem, because of its energy spreading out in time. The peak is so low that it is hardly detectable at all. One solution is a wider averaging to hope for the signal to raise above the noise. This problem is depicted in Figure 5.3 where the signal in the uppermost row is very noisy compared to the signal on the lowermost row. The classification of these test pairs goes as the Figure 5.4 where the lighter areas mean a lower error and therefore a more probable result.

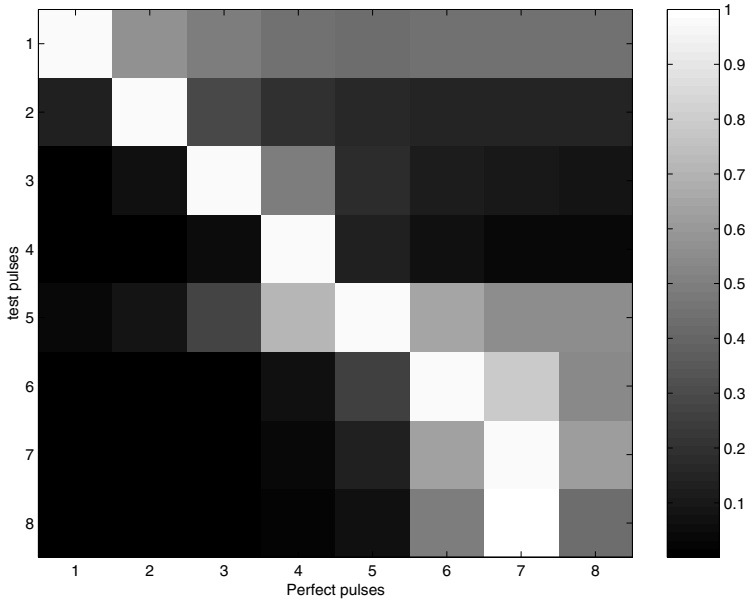

Figure 5.4. The resulting classification. Analogue to Figure 5.3 each row is one test signal where, for example, the last test signal is detected as the seventh class, which is an incorrect classification. White means the most probable and black means not probable at all.

This method was tried on a set of 3-D laser radar data and the result is shown in Figure 5.6. In this case the target was a simple handmade lorry consisting of four boxes, as in Figure 5.5. This result should be compared to the perfect result shown in Figure 5.7. The vertical black line in the middle of Figure 5.6 represents the gap between the wheel house and the platform on the lorry and should not be considered as an error.

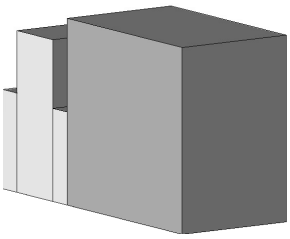

Figure 5.5. The lorry consisting of four boxes used during the slope estimation test.

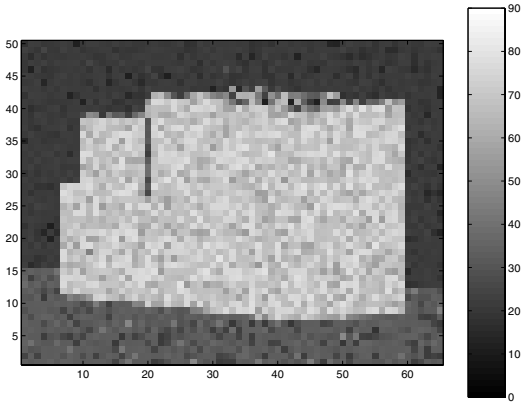

Figure 5.6. The resulting estimated angle of each pixel of the ordinary lorry. Compare the result to Figure 5.7.

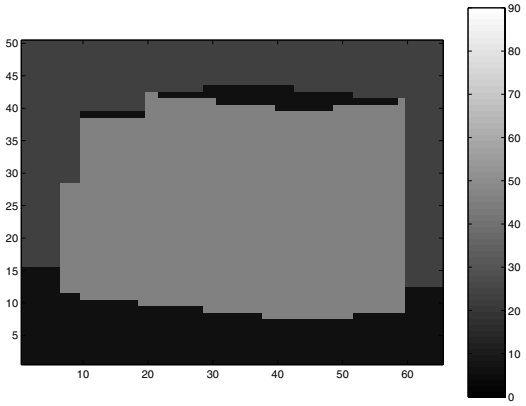

Figure 5.7. The correct angles in each pixel.

5.3 Surface identification

5.3.1 Plane surface

A plane surface can very well be identified by the afore mentioned technique, as long as the noise level is rather low. Too steep slopes are still a problem, where the reflected signal is so weak that it disappears in the noise. Even if the SNR is high enough to detect the signal, the noise will affect the signal so much that it cannot be identified correctly. This can be viewed in Figure 5.6, on the roof of the lorry. A disadvantage with the standard laser radar equipment instrumentation is that it is impossible to detect the direction of the slope, as long as the beam is radial symmetric.

5.3.2 Corner

Corners, both inner and outer, are difficult to identify, since the only way the pulse characteristics will change is that the pulse will change its width. It will therefore be identified as one sloping surface, with the wrong angle estimation, instead of two different slopes.

5.3.3 Step

A step means two, or more, separate surfaces at different distances. If the surfaces are separated enough to keep the reflected pulses separated, there will be no problem detecting and identifying them both, though its impossible to determine where in the beam the different surfaces appear.

5.4 Possible problems of classification

To conclude the problems with classification, the first thing to mention must be the noise. If the SNR is too low the smoothing is unavoidable and makes the signal appear more clear and makes it easier to detect. But the noise also makes the pulse wider and the pulse is therefore detected as a pulse with a too heavy slope.

The second source of error is the different kinds of target structures. For instance, a corner would be detected as a plane surface with wrong slope as mentioned above.

5.5 Some ideas concerning detection in noise

5.5.1 Smoothed maximum method

The first technique used here for positioning the maxima of the pulses in a signal is a straight forward technique, where the signal is smoothed by an averaging filter followed by threshold. This thresholding extracts a few areas of interest and if each area is big enough to contain the smallest possible pulse, the maximum peak inside each area is calculated. These maxima are considered to be the maxima of different target reflections, and if there are more than one maximum, the target is considered consisting of a step, see section 5.3.3.

The maximum values are considered to be the maximum of the reflected signal, though this may not be true in reality. In fact, the calculated time for the maxima often do not correspond to the correct maxima time, mostly due to noise, and this case is shown in Figure 5.8, where the maximum of the correct pulse (dashed line) lies at about $2.65 \cdot 10^{-7}$ and maximum of the noisy signal (slightly smoothed) lies at about $2.67 \cdot 10^{-7}$ (noisy line in Figure 5.8 and dashed line in Figure 5.9).

This small disparity in time (between the two dashed lines in the Figures 5.8 and 5.9) may not be a problem but becomes one when surface recognition is performed on the pulse. To identify the pulse correctly the surface templates have to lie exactly above the unknown pulse, or the pulse will be detected as a wider pulse, than it really is.

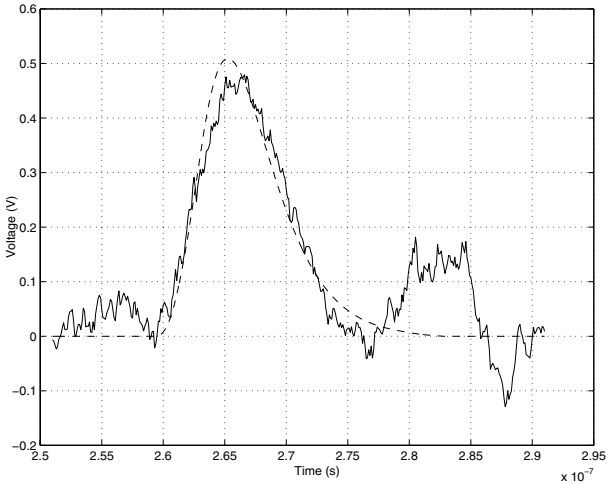

Figure 5.8. The smoothed original signal and the template pulse (dashed).

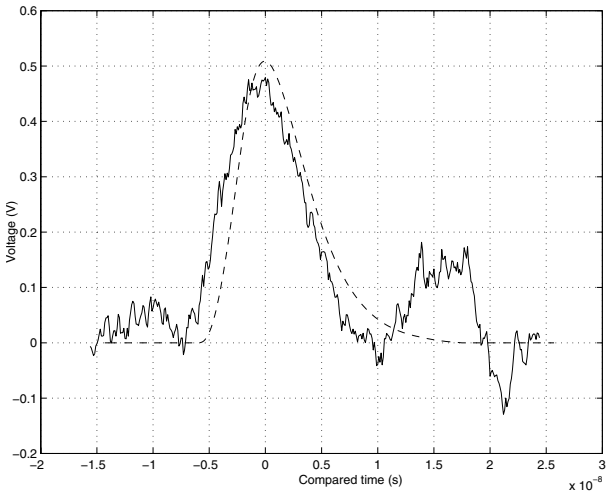

Figure 5.9. The smoothed original signal and the result of the *smoothed maximum method*. The estimated signal (dashed) does not correspond to the correct one in Figure 5.8.

5.5.2 Correlation method

As in Danielsson [3], a better method for finding a certain pattern in a signal is to look at the correlation between the signal and the template pattern. The correlation is applied as

$$c(t) = (s_{\text{template}} \,\square\, p)(t) = \sum_{i=0}^{n} s_{\text{template},i} \cdot p_i(t), \tag{5.2}$$

where n is the length of the template pattern $s(t)$, and $p(t)$ is the unknown test signal.

If the pattern somewhere coincides with the signal a peak will occur in the correlation and this peak will, in contrast to the smoothed maximum method, be placed on a more probable position since it looks at the best fit for the waveform along the signal. The same example pulse as in the smoothed maximum method would give a correlation curve like Figure 5.10, where the peak is placed more correctly. Figure 5.11 shows where the pulse would be placed in the surface recognition. It is almost the same place as the original correct pulse in Figure 5.8.

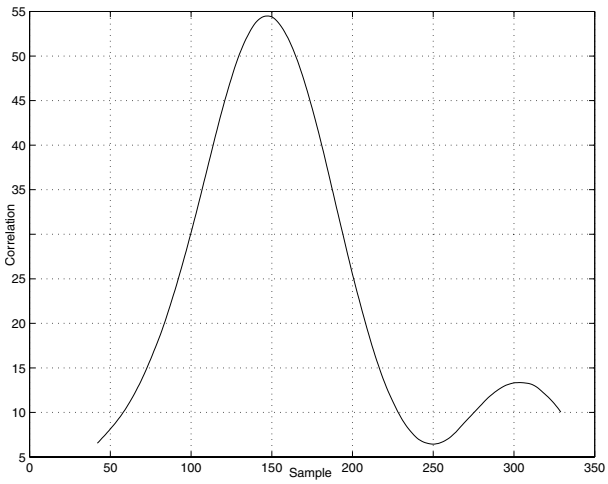

Figure 5.10. The correlation curve for the previous example. The peak appears where the template pulse best fits the noisy pulse.

In this case the problem is to know which template pulse to test, since each template would give different correlation results. The template that best matches the original pulse is the one that best would identify the maximum. Unfortunately, the shape of the original pulse is unknown, but if a set of template pulses with different widths are created, each and every signal can be detected. A third alternative is to combine these two methods, to get a more reliable method, but this has not been tested in this report.

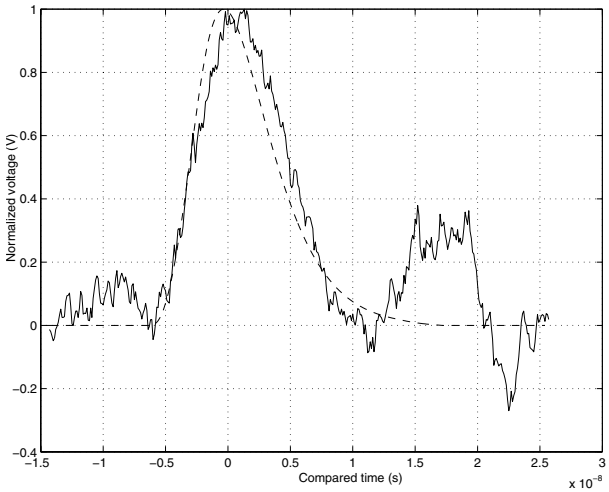

Figure 5.11. The result of the *correlation method*. The estimated signal (dashed) almost overlaps the correct one in Figure 5.8.

6 Simulation results

The implemented simulation algorithms give the opportunity to test the capacity of a scanning 3-D laser radar. It also provides a good possibility to get an intuitive understanding how different parameters in the environment affects the result. This section presents some simulations while changing only one parameter at a time. The simulations presented in this report are different target geometries, effects of different reflection properties, atmospheric attenuation effects, different kinds of detection algorithms and for the case of scanning 3-D laser radar, different sizes of scanning arrays.

6.1 Different target geometries

The first simulation presented is a reflection at a step illuminated and seen from several different angles, see left part of Figure 6.1. The resulting waveforms are presented to the right in Figure 6.1. Note that while the elevation angle is small the reflection gives a double pulse response.

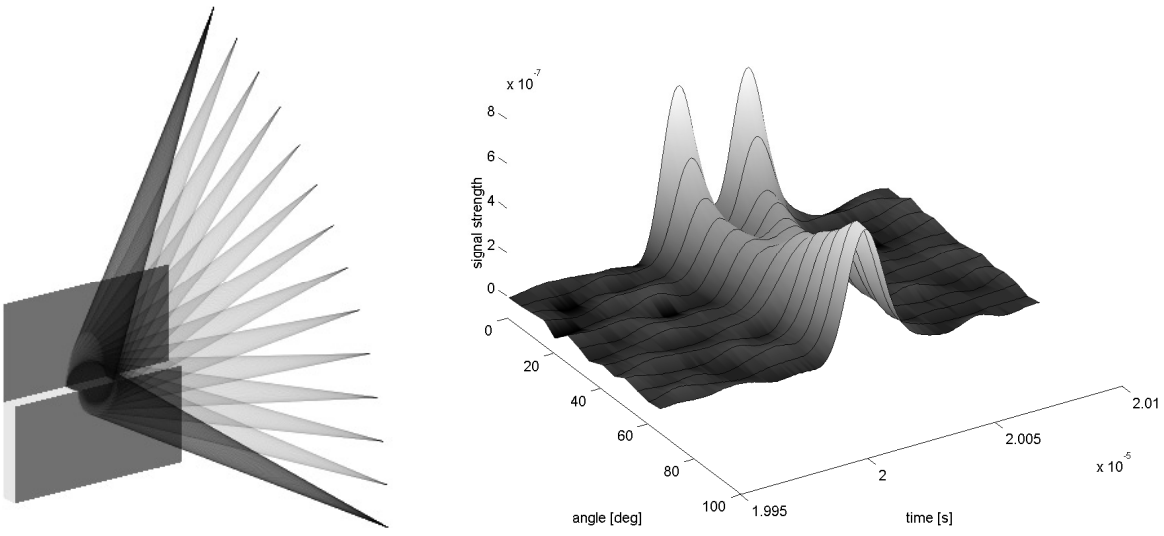

Figure 6.1. The geometric step illuminated from different points of view. The angle represents the different elevations

6.2 Reflection properties

Two different reflection conditions have been modeled and they are rendered in Figure 6.2, describing a helicopter, where the left image has a large specular part in the reflection while the right image only has a diffuse part of the reflection. The images describe the peak power in the reflected waveform. The parameters for the BRDF calculations used in the simulations in Figure 6.2 were, corresponding to the assignments introduced in section 2.2.2, for the left image A=1, B=0.25, m=1 and s=0.1, and for the right simulation A=0, B=0.5, m=1 and s is arbitrary.

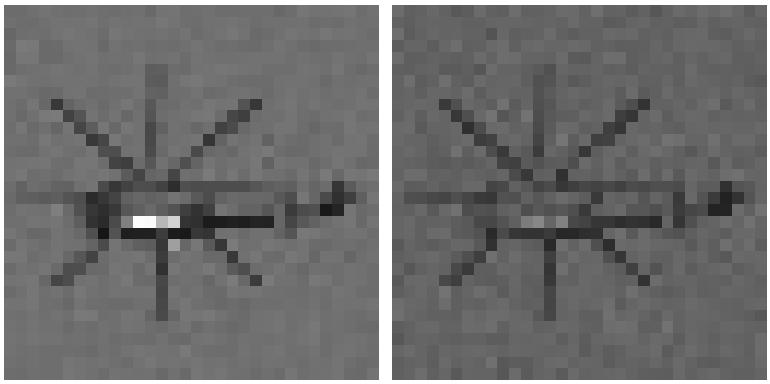

Figure 6.2. Two different settings of the reflection. To the left the specular reflection is strong and to the right the reflection is purely diffuse. The perpendicular part of the helicopter gives a stronger reflection in the specular case (the light spots in the left figure).

6.3 Atmospheric attenuation

At long distances to the target, the signal would be attenuated due to the atmosphere and fade into noise. In Figure 6.3, the target is placed at a distance of 10 km and the visibility is changed (from 6 to 15 km). It is obvious that the signal is easier to detect when the visibility increases. The parameters used in the simulations below are constant (except for the visibility) where the laser pulse energy $E_p = 1$ mJ, the pulse width $T_{1/2} = 5$ ns, the wavelength $\lambda = 1060$ nm and the number of pixels in the scanning array were 32×32. The noise-equivalent-power (NEP, the standard deviation for the noise) were constant at about 15 nW, while the peak power from the laser radar reflected at the target changed from 10 nW for 6 km visibility to 550 nW for 15 km visibility.

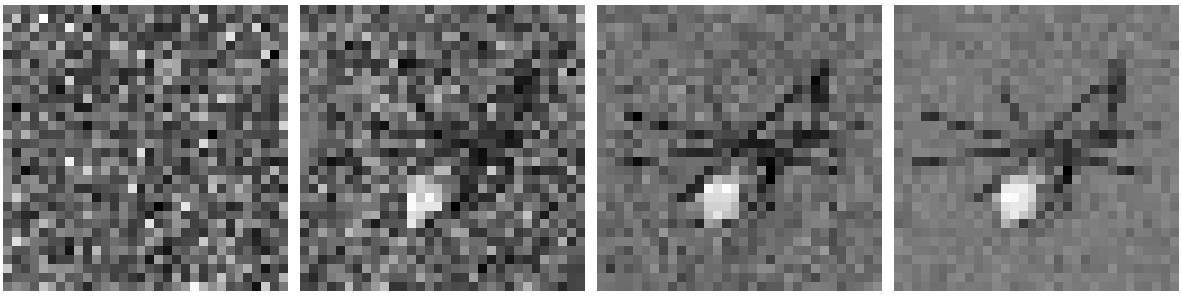

Figure 6.3. Example of maximum pulse response when the visibility is changed from 6 to 15 km. From left to right the visibility is 6, 8, 10 and 15 km, respectively.

6.4 Different detection algorithms

When determining the range to a target an important part is the detection of the return pulse. There are several ways of detecting the pulse and two of them will be exemplified in this report: peak detection and 50 % leading edge detection, see Figure 6.4. Figure 6.5 shows an example of a tank at 3 km distance with high signal-to-noise-ratio (SNR) detected with the two different detection techniques. Notice that the barrel of the tank is detected with the 50 % leading edge detection technique but not with the peak detection technique. The corresponding waveform is presented in Figure 6.4 where the detected distances are marked with stars. The peak detection detects the highest peak while the leading edge detection detects the rising edge at half peak power. Since the first peak is lower than the second, the detection method detects different return pulses. Leading edge detection recognizes the barrel while the peak detection detects the ground behind the barrel. The parameters used in the simulation are the same as in the earlier example, see Figure 6.3, except from the pulse width $T_{1/2}$ which in this case is set to 19 ns. The visibility is 5 km. Even in this case, the NEP is about 15 nW.

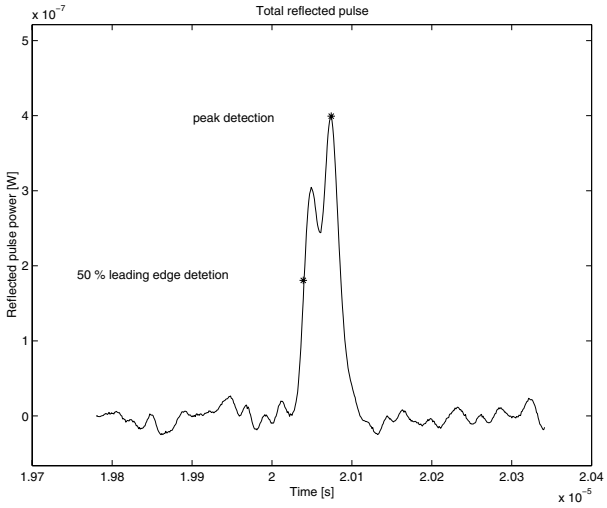

Figure 6.4. Two different pulse detection algorithms used in laser radar systems. The detected distances are marked by stars. The left pulse peak is the response from the barrel while the right pulse peak is from the ground behind the tank.

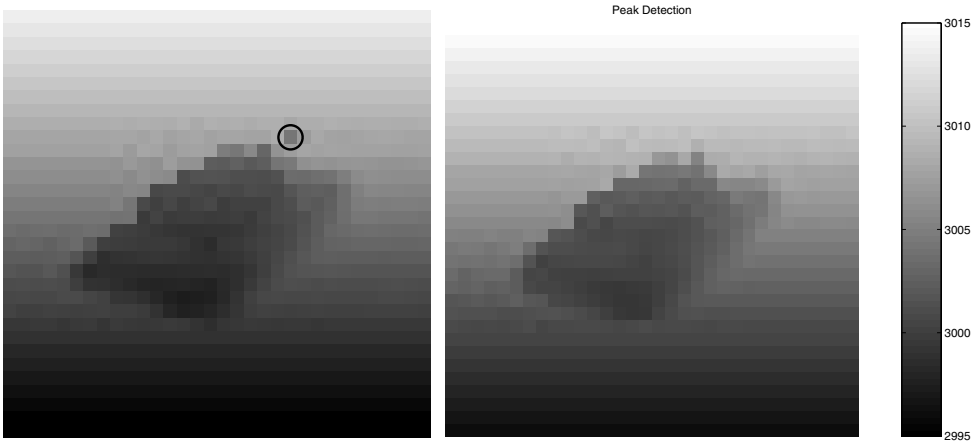

Figure 6.5. Two distance images with different detection techniques. The barrel is marked by a circle.

6.5 Different number of laser image pixels on target

In a scanning laser radar a laser beam scans the target in a predefined pattern, for example a 10×10 pixel square. The distance between these pixels at the target depends on the range to the target, and is usually about the size of the laser beam diameter. To give an example of two different scanning arrays sizes Figure 6.6 describes the same target with the only difference as the density of the pixels. All settings are the same as in section 6.4.

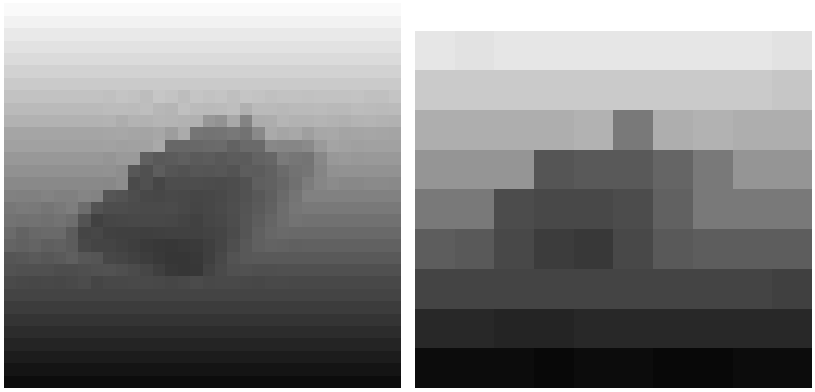

Figure 6.6. Two distance images from scans over the same target tank with different scan density.

6.6 Conclusions

The target imaging requires a modeling tool, which can predict the performance and result from a laser radar system. The presented model is a first step in that direction and will provide the possibility to estimate the limits of the laser radar equipment of today and tomorrow. The model has so far given interesting results but has to be refined and validated by comparing with experimental results. Further development and adaptations to different kinds of laser systems will be made, for example to coherent systems and gated viewing systems.

7 Conclusions & future work

7.1 Conclusions

The validation did not completely fulfill the requirements of a proper validation, although the measured data seemed to follow the rules that were implemented in the simulation tool. Since the same algorithms have been accepted by scientists around the world, the conclusion is that the toolbox is valid enough.

The target recognition appeared to give very good results. For reasonable noise levels, the classification showed to be stable. However, the data used for the classification were taken from the simulation program, which did not include any unknown parameter. If the classification is to be made on real, measured data, some parameters could be unknown and the resulting classification would give worse results. This may not be a problem though, because the most important factor when classifying a surface slope, is the pulse length $T_{1/2}$, which is a well known parameter in a laser radar system.

7.2 Toolbox extensions

An obvious area of extensions is the MATLAB toolbox where many functions easily can be added. For instance functions that connect the present toolbox functions and make the toolbox simpler and more efficient to use. As implemented now, most of the functions work independently.

Gated Viewing could be included, see the SPIE paper [15] for more information. To do this only some additional noise algorithms and a few functions need to be added.

7.3 Surface classification extensions

The surface classification treated in this report must be considered quite simple. There are many extensions in this field. For example, the information about the slope in each subarea of a laser radar image could tell even more about the surface, and a reconstruction would be a much more correct image of the target. Edges (detected as double pulses) can be detected and also included into the representation.

The next step could be to classify the targets into different groups, e.g. tanks, lorries and trees. The advantage of using the implemented surface classification is that since we could get a more correct target description, this classification would be more exact and less dependent on a low noise level. An even more advanced step (and also even more interesting) would be to identify what kind of tank we see through our laser radar system.

There are reports from studies about target recognition without any kind of surface classification. The classification is made from information about the depth only. A combination

between this report and a further classification, see for example Der et al. [5], can possibly result in a better classification.

Another interesting study has been performed by Holmes et al. [8], and covers some ideas to use multifeature analysis. They used up to 90 (!) features from the targets, such as Fourier descriptor, energy, entropy, area moment invariant and autocorrelation, and achieved a 100 % target recognition. Maybe this is considered an overkill...

Finally, a work done by Bhattacharya et al. [1], analyses waveform from *Lidar* (light detection and ranging). Through neural network theories, the data is classified and a pulse can be identified as belonging to a specific class. Neural network fundamentals can be studied in Haykin [7].

References

[1] D. Bhattacharya, S. R. Pillai, and A. Antoniou. Waveform classification and information extraction from lidar data by neural networks. *IEEE Transactions on Geoscience and Remote Sensing*, 35(3):699–707, May 1997. ISSN: 0196-2892.

[2] Burle Industries Inc., Lancaster, PA, USA. *Electro-Optics Handbook*, 1992.

[3] P-E. Danielsson, O. Seger, and M. Magnusson Seger. Bildbehandling. Department of Electrical Engineering, Linköping University, Linköping, Sweden, 1999. Course Compendium in Swedish.

[4] S. Der, B. Redman, and R. Chellappa. Simulation of error in optical radar range measurements. *Applied Optics*, 36(27):6869–6874, September 1997.

[5] S. Der, Q. Zheng, and R. Chellappa. Model-based target recognition in pulsed ladar imagery. *IEEE Computer Society Conference on Computer Vision and Pattern Recognition*, pages 515–520, June 1998. ISBN: 0-8186-8497-6.

[6] C. Fox, J. Accetta, and D. Shumaker, editors. *The Infrared and Electro-Optical Systems Handbook*, volume 6. SPIE Optical Engineering Press, Bellingham, Washington, USA, 1994. Subtitle: *Active Electro-Optical Systems.*

[7] S. Haykin. *Neural networks, a comprehensive foundation.* Prentice Hall, Upper Saddle River, New Jersey 07458, 2nd edition, 1999.

[8] Q. A. Holmes, X. Zhang, and D. Zhao. Multiresolution surface feature analysis for automatic target identifaction based on laser radar images. In *Proceedings of the International Conference on Image Processing*, volume 3, pages 468–471, Environ. Res. Inst. of Michigan, Ann Arbor, MI, USA, October 1997. (IEEE). ISBN: 0-8186-8183-7.

[9] The MathWorks, Inc., Cochituate Place, Natick, MA. USA. *MATLAB: Using MATLAB Graphics*, 1996.

[10] Optech Inc., 701 Petrolia Road, Downsview, Ontario, Canada. *Optech Rangefinder 501SX Operating Manual*, March 1987.

[11] M. I. Skolnik. *Radar Handbook.* McGraw-Hill, New York, 2nd edition, 1990.

[12] O. Steinvall. Theory for laser systems performance modelling. Technical Report FOA-R--97-00599-612--SE, Div. of Sensor Technology, Defence Research Establishment (FOA), Sweden, Oct 1997.

[13] O. Steinvall. Effects of target shape and reflection on laser radar cross sections. Technical Report FOA-R--99-01201-408,612--SE, Div. of Sensor Technology, Defence Research Establishment (FOA), Sweden, Sept 1999.

[14] O. Steinvall. Waveform simulation for 3-d sensing laser radars. Technical Report FOA-R--00-01530-612,408--SE, Div. of Sensor Technology, Defence Research Establishment (FOA), Sweden, May 2000.

[15] O. Steinvall, H. Olsson, G. Bolander, C. Carlsson, and D. Letalick. Gated viewing for target detection and target recognition. In *Proceedings of the 4th (SPIE) Symposium on Laser radar Technology and Applications*, volume 3707, pages 432–448, Orlando, Florida and Munich, Germany, April and June 1999. (SPIE).

Appendix A: Toolbox

This appendix contains descriptions of the MATLAB toolbox functions for simulating 3-D laser radar waveforms. The equations implemented in the toolbox functions are listed, followed by the purpose for the function. The toolbox functions are:

Function name	Description
`aerial_attenuation`	The atmospheric attenuation due to particles in the air
`background_illumination`	Background illumination induced noise current
`beam_broadening`	Beam broadening due to turbulence
`beam_energy_distribution`	Laser beam irradiance distribution and total power
`create_pulse`	Laser beam radial distribution, with concern to both speckle and turbulence
`detector_noise`	Noise equivalent power (NEP) from detector
`exp_pulse_propagation`	Laser pulse time propagation
`laser_system_scaling`	Laser system scale factor according to aerial attenuation, system efficiency and signal peak power
`pdfrand`	Random number generator, given a certain PDF
`simple_BRDF`	BRDF calculations for known BRDF parameters
`speckle_pdf`	The PDF for the speckle modulation
`turbulence_cell_radius`	Radius of turbulence scintillation cells
`turbulence_pdf`	The PDF for the turbulence scintillation
`turbulence_scintillation`	Standard deviation for the turbulence scintillations

`aerial_attenuation`

Syntax:
`[sigma_aer]=aerial_attenuation(VM, lambda)`

Function:
$\sigma_{\text{aer}} = \frac{3.91}{V_{\text{M}}} \left(\frac{\lambda}{0.55}\right)^{-q}$

$q = f(V_M)$

Explanation:
Aerosol attenuation. The particles in the air make the beam fade out during long flights. This expression is only valid if the wavelength is between 0.4 and 2 μm.
Section 2.3.3.

`background_illumination`

Syntax:
`Ib=background_illumination(rho, h_sun, Tr, Aa, theta_fov, delta_lambda)`

Function:
$I_{\text{b}} = \Re P_{\text{b}} = \Re \varrho_{\text{refl}} h_{\text{sun}} T_{\text{r}} A_{\text{a}} \sin\left((\frac{\vartheta_{\text{fov}}}{2})\right)^2 \Delta\lambda$

Explanation:
Current induced into the receiver from the background illumination.
Section 2.4.

`beam_broadening`

Syntax:
`[w_lt, w_st]=beam_broadening(Cn, R, w, w0, lambda)`

Function:
$w_{\text{lt}} = w \cdot \left(1 + 1.624 \cdot (\sigma^2_{\text{Rytov}})^{6/5} \cdot \Lambda_1\right)^{1/2}$

$w_{\text{st}} = w \cdot \left(1 + 1.33 \cdot \sigma^2_{\text{Rytov}} \cdot \Lambda_1^{5/6} - 1.04 \cdot \sigma^2_{\text{Rytov}} \cdot \Lambda_1 \cdot \Lambda_0^{1/6}\right)^{1/2}$

$\sigma^2_{\text{Rytov}} = 1.23 \cdot C^2_{\text{n}} \cdot k^{7/6} \cdot R^{11/6}$

$\Lambda_1 = \frac{\lambda R}{\pi w^2}$

$\Lambda_0 = \frac{\lambda R}{\pi w_0^2}$

Explanation:
Turbulence increases the beam radius according to this rules.
Section 2.3.1.

`beam_energy_distribution`
Syntax: `[beam_radius, irradiance_distribution, power]= beam_energy_distribution(lambda, phi, R, R0, r_vector)`
Function: $I(r) = \left(\frac{w_0}{w}\right)^2 \cdot e^{-\frac{2r^2}{w^2}}$ $P_{\text{tot}} = \int_0^\infty I(r) \cdot 2\pi r \, \mathrm{d}r = \frac{\pi w_0^2}{2}$ $w = w_0 \cdot (\Omega_0^2 + \Omega^2)^{0.5}$ $w_0 = \frac{2\lambda}{\pi\phi}$ $\Omega = \frac{\lambda R}{\pi w_0^2}$ $\Omega_0 = 1 - \frac{R}{R_0}$
Explanation: The beam energy radial distribution and the total pulse energy. Section 2.1.2.

`create_pulse`
Syntax: `[P_sp_tot, P_turb_tot, beam_distr]=create_pulse(x_min, x_max, y_min, y_max, part_resolution, beam_separation, Cn, R, R0, wo, r_target, phi, IFOV, lambda, x_centre, y_centre)`
Explanation: The beam energy spatial distribution. Since too many mathematical functions is used to create the spatial radial distribution these are not resented here. Mostly other toolbox functions are used throughout the creation process.

`detector_noise`
Syntax: `Noise_power_det=detector_noise(e, B, Ids, Iampl, Idb, Ib, Is, Mg, F, R_esp)`
Function: $\text{NEP}_{\text{detector}} = \frac{(2e_{\text{c}}B \cdot (I_{\text{ds}} + (I_{\text{db}} + I_{\text{b}} + I_{\text{s}})M^2F))^{1/2}}{\Re}$
Explanation: Noise equivalent power. The standard deviation for the noise in the detector. Section 2.4.

`exp_pulse_propagation`
Syntax: `laser_pulse=exp_pulse_propagation(T_half,timevector)`
Function: $p(t) = \left(\frac{t}{\tau}\right)^2 \cdot e^{-\frac{t}{\tau}}$ $\tau = T_{1/2}/3.5$
Explanation: Laser pulse time propagation. Section 2.1.1.

`laser_system_scaling`
Syntax: `Scale_factor=laser_system_scaling(eta_syst, Ep, tau, sigma, R)`
Function: $S = \eta_{\text{syst}} \frac{E_\text{p}}{2\tau} \cdot e^{-2\sigma R}$
Explanation: Receiver peak power factor scales the signal in addition to the air attenuation. Section 2.5.2

`pdfrand`
Syntax: `Random_S=pdfrand(PDF, S, number_of_times)`
Explanation: Given a certain PDF, a random number is generated. Since the functions used has no connection to the laser radar theory, they are not listed here.

`simple_BRDF`
Syntax: `rho_b=simple_BRDF(A,B,m,theta,s)`
Function: $\boldsymbol{\rho} = \boldsymbol{\rho}_{\text{spec}} + \boldsymbol{\rho}_{\text{diff}} = \frac{A}{\cos^6(\theta)} e^{-\frac{\tan^2(\theta)}{s^2}} + B\cos^m(\theta)$
Explanation: Bidirectional reflection distribution function. Section 2.2.2.

`speckle_pdf`

Syntax:

`[S, P_dir_M]=speckle_pdf(lambda, phi, D_rec)`

Function:

$$P_{\mathrm{dir,M}}(S) = \frac{\left(\frac{M}{S_{\mathrm{av}}}\right)^{M} S^{M-1} \cdot e^{-M\frac{S}{S_{\mathrm{av}}}}}{\Gamma(M)}$$

$$M = \frac{D_{\mathrm{rec}}}{D_{\mathrm{sp}}}$$

$$D_{\mathrm{sp}} = \frac{\lambda}{\phi}$$

Explanation:

The pdf for the speckle amplitude modification. The return signal, `S`, contains the multiplicators and `pdf_dir_M` contains the probability of each corresponding multiplicator. Section 2.2.3.

`turbulence_cell_radius`

Syntax:

`rho_l=turbulence_cell_radius(Cn, R, wo, phi, lambda)`

Function:

$$\rho_{\mathrm{l}} = \frac{\sqrt{\frac{R}{k}}}{\sqrt{1+\frac{R}{k\rho_0^2}}}$$

$$\rho_0 = \rho_{0,\mathrm{p}} \cdot \left(\frac{\left(1-\frac{R}{f}\right)^2 + \left(\frac{R}{z_{\mathrm{B}}}\right)^2 (1+\frac{\delta^2}{3}) \cdot \frac{1}{1+\delta^2}}{1-\frac{13R}{3f}+\frac{11}{3}\left(\frac{R}{f}\right)^2+\frac{1}{3}\left(\frac{R}{z_{\mathrm{B}}}\right)^2+\frac{1}{3}\left(\frac{R}{f}\right)^2 \cdot \frac{1+\frac{\delta^2}{4}}{1+\delta^2}} \right)^{1/2}$$

$$\rho_{0,\mathrm{p}} = (1.46 \cdot k^2 C_{\mathrm{n}}^2 R)^{-3/5} \quad z_{\mathrm{B}} = \left(\frac{kw_0}{2}\right) \cdot \left(\frac{1}{\rho_{0,\mathrm{s}}^2} + \frac{1}{4w_0^2}\right)^{-1/2}$$

$$\rho_{0,\mathrm{s}} = (0.5 \cdot k^2 C_{\mathrm{n}}^2 R)^{-3/5}$$

$$f = \frac{-w_0}{\tan(\frac{\phi}{2}) - \tan(\frac{\lambda}{2\pi w_0})}$$

$$\delta = \frac{2w_0}{\rho_{0,\mathrm{p}}}$$

Explanation:

The cell radius of the turbulence scintillation.
Section 2.3.2.

`turbulence_pdf`

Syntax:
`[S, pdf_scint]=turbulence_pdf(sigma2_target)`

Function:

$$p_{\text{scint}} = \frac{1}{S \cdot \sqrt{2\pi\sigma^2_{\ln I}}} \; e^{-\left(\frac{\left(\ln(\frac{S}{S_{\text{av}}}) + \frac{1}{2}\sigma^2_{\ln I}\right)^2}{2\sigma^2_{\ln I}} \right)}$$

$$\sigma^2_{\ln I} = \ln(1+\sigma_I^2) = \ln(1+\sigma^2_{\text{target}})$$

Explanation:
The pdf for the turbulence scintillation amplitude. The return signal, `S`, contains the multiplicators and `pdf_scint` contains the probability of each corresponding multiplicator.
Section 2.3.2.

`turbulence_scintillation`

Syntax:
`[sigma2_target, rho_l, r_eff]=turbulence_scintillation(Cn, R, R0, wo, r_target, phi, IFOV, lambda)`

Function:

$$\sigma^2_{\text{target}} = \gamma \cdot \sigma^2_{\text{sat,point}}$$

$$\sigma^2_{\text{sat,point}} = \frac{1.3 \cdot \sigma^2_{\text{point}}}{1+\sigma^2_{\text{point}}}$$

$$\sigma^2_{\text{point}} = 1.23 \cdot C_{\text{n}}^2 \cdot k^{7/6} \cdot (2R)^{11/6}$$

$$\gamma_{\text{target}} = \left(\frac{\rho_{\text{l}}}{r_{\text{eff}}}\right)^{7/3}$$

$$r_{\text{eff}} = min(r_{\text{target}},\ w,\ \frac{\vartheta_{\text{fov}}}{2} \cdot R)$$

Explanation:
The normalized variance of the turbulence scintillation amplitude.
Section 2.3.2.

Index

Bold numbers mean the definition of or explanation for the word.

Italic numbers refer to figures illustrating the word.